Analysis of European ozone trends in the period 1995–2014

Yingying Yan[1,2,3], Andrea Pozzer[1], Narendra Ojha[1], Jintai Lin[2], Jos Lelieveld[1]

[1] Atmospheric Chemistry Department, Max Planck Institute for Chemistry, Mainz, Germany

[2] Laboratory for Climate and Ocean-Atmosphere Studies, Department of Atmospheric and Oceanic Sciences, School of Physics, Peking University, Beijing 100871, China

[3] Department of Atmospheric Sciences, School of Environmental Studies, China University of Geosciences (Wuhan), 430074, Wuhan, China

Email: andrea.pozzer@mpic.de

Abstract

Surface-based measurements from the EMEP and Airbase networks are used to estimate the changes in surface ozone levels during the 1995–2014 period over Europe. We find significant ozone enhancements (0.20–0.59 $\mu g/m^3$/y for the annual means; P-value < 0.01 according to an F-test) over the European suburban and urban stations during 1995–2012 based on the Airbase sites. For European background ozone observed at EMEP sites, it is shown that a significantly decreasing trend in the 95th percentile ozone concentrations has occurred, especially during noontime (0.9 $\mu g/m^3$/y; P-value < 0.01), while the 5th percentile ozone concentrations continued to increase with a trend of 0.3 $\mu g/m^3$/y (P-value < 0.01) during the study period. With the help of numerical simulations performed with the global chemistry-climate model EMAC, the importance of anthropogenic emissions changes in determining these changes over background sites are investigated. The EMAC model is found to successfully capture the observed temporal variability in mean ozone concentrations, as well as the contrast in the trends of 95th and 5th percentile ozone over Europe. Sensitivity simulations and statistical analysis show that a decrease in European anthropogenic emissions had contrasting effects on surface ozone trends between the 95th and 5th percentile levels, and that background ozone levels have been influenced by hemispheric transport, while climate variability generally regulated the inter-annual variations of surface ozone in Europe.

1. Introduction

Tropospheric ozone has detrimental effects on human health, and elevated concentrations at the surface are of concern over most of the European region (Hjellbrekke and Solberg, 2002; WHO, 2013; EEA, 2013; Lelieveld et al., 2015). The European Union (EU) Air Quality Directive sets four standards for surface ozone to reduce its impacts on human health and crop yields (http://eur-lex.europa.eu/legal-content/EN/TXT/HTML/?uri=CELEX:32008L0050&from=EN). These standards are: information threshold (1-hour average: 180 $\mu g/m^3$), alert threshold (1-hour average: 240 $\mu g/m^3$), long-term objective (maximum diurnal 8-hour mean: 120 $\mu g/m^3$), and the

35 target value (long-term objective that should not be exceeded more than 25 days per year,
36 averaged over 3 years). Exceedances are particularly frequent in regions close to high ozone
37 precursor emissions during summer with stagnant meteorological conditions, associated with
38 persistent high temperatures. Since a substantial decrease in precursor concentrations has been
39 achieved in Europe in recent decades, the number of exceedances has declined (Guerreiro et al.,
40 2014), in line with a long-term downward trend of pollution emissions (Colette et al., 2011;
41 Wilson et al., 2012). Further, a number of studies has shown that European ozone levels are on
42 average decreasing in the last 20 years (as example, Jonson et al, 2010). Nevertheless,
43 background ozone changes over Europe are not so clear (Wilson et al., 2012), being sensitive to
44 climate conditions and intercontinental transport of O_3 and its precursors, and are significant in
45 view of tropospheric chemistry (Lelieveld and Dentener, 2000; Lawrence and Lelieveld, 2010).

46 The response of surface ozone to a changing climate, with potentially more frequent heat
47 extremes (Bloomer et al., 2009; Jacob and Winner, 2009; Cooper et al., 2012; Fu et al., 2015; Lin
48 et al., 2015; Simon et al., 2015), and concurrent changes in anthropogenic emissions of precursor
49 gases (Bloomer et al., 2009; Fu et al., 2015; Strode et al., 2015; Yan et al., 2018) may pose a
50 challenge for air quality management. Observation and model-based analyses of ozone trends in
51 responses to climate change (Bloomer et al., 2009), precursor emissions (Bloomer et al., 2009;
52 Lefohn et al., 2010), and long-range transport (Lin et al., 2015) have been conducted for North
53 America (Strode et al., 2015; Lin et al., 2017; Yan et al., 2018), several Asian regions (Brown-
54 Steiner et al., 2015; Lin et al., 2017) and also for Europe (Meleux et al., 2007, Wilson et al.,
55 2012, Jonson et al., 2006). For Europe, the connection between climate and ozone levels has been
56 subject of large number of studies, notably to investigate the effects of climate change on surface
57 ozone levels (Langner et al., 2005; Meleux et al., 2007; Colette et al., 2011; Langner et al., 2012.)

58 Tropospheric ozone is produced photochemically during daytime, mainly from the photolysis of
59 nitrogen dioxide (NO_2), while NO_2 levels are strongly influenced by radicals and their precursors,
60 including organic compounds. Due to the complex photo-chemistry involved, the amount of
61 ozone formed responds nonlinearly to changes in precursor emissions and is sensitive to
62 variations in air temperature, radiation and other climatic factors (Fu et al., 2015; Monks et al.,
63 2015; Coates et al., 2016). Ozone can be destroyed via reaction with NO (i.e., ozone titration)
64 especially during nighttime, and thus a reduction in NO_x emissions could result in more ozone
65 (Jhun et al., 2014; Yan et al., 2018). Previous studies of European ozone have focused on daytime
66 or diurnal mean ozone with little attention paid to the daytime-nighttime contrast in ozone
67 changes (Colette et al., 2011; Wilson et al., 2012; Guerreiro et al., 2014).

68 Our work contrasts the trends of the monthly 5th and 95th percentile European background ozone
69 levels at hourly levels over the period 1995–2014, based on the hourly ozone measurements from
70 the EMEP network. Additionally, numerical simulations from the global chemistry-climate
71 model ECHAM5/MESSy (EMAC) are conducted to evaluate the model's ability in capturing
72 ozone trends over Europe and to investigate the underlying importance of the meteorology and
73 emission changes for the observed ozone trends.

74 The manuscript is organized as follows: the observational dataset, model simulations and analysis
75 methods are described in Section 2. In Section 3, the average linear trends for the European
76 domain are estimated and analyzed separately for the monthly, seasonal and annual 5th, 50th, and
77 95th percentiles of the observed surface ozone concentrations. We then compare the observed
78 ozone trends and variability to results of the atmospheric chemistry – general circulation model
79 EMAC. To investigate the effects of anthropogenic emissions and climate variability on observed
80 European ozone changes, we conduct a sensitivity simulation with constant emissions and
81 statistical analysis with the ERA-Interim 2-meter temperature data in Section 4. Followed by the
82 conclusions in Section 5.

83 **2. Methods and Data**

84 **2.1 Ozone measurements**

85 The hourly ground-level ozone measurements over 1995–2014 have been obtained from the
86 Chemical Coordination Centre of *European Monitoring and Evaluation Programme (*EMEP)
87 network (http://www.nilu.no/projects/ccc/emepdata.html). Table 1 shows the number of
88 measurement sites (varies from 113 to 137) and the percentage of missing hourly data in each
89 year. Fig. 1 further shows the site distribution. Since many of the stations are not operating
90 continuously during the study period (Fig. 1), we have included only the sites in the analysis
91 which fulfill the criteria defined by Cooper et al. (2012). Such data selection criteria are further
92 applied for the US ozone trends analysis with the EPA-AQS measurements by Yan et al. (2018).
93 First, we discard the observational days with the valid hourly data less than 66.7% in any daytime
94 or nighttime. Then, we discard the particular season with less than 60 days containing valid data
95 in any season. Finally, for any season, we keep the data with valid seasonal mean ozone more
96 than 15 years during 1995–2014; otherwise we discard the data in all years for the particular
97 season. Fig. 1 shows the final selected 93 sites satisfying above criteria for the analysis.

98 As the measurements from EMEP network are carried out under the "Co-operative programme
99 for monitoring and evaluation of the long-range transmission of air pollutants in Europe", the
100 monitoring sites are located where there are minimal local influences, and consequently the
101 observations are representative of relatively large regions (Torseth et al., 2012). In order to
102 compare the observed ozone levels and changes over urban, suburban and rural sites, we also use
103 the hourly measurements over 1995–2012 from the European Environment Agency Airbase
104 system (https://www.eea.europa.eu/data-and-maps/data/airbase-the-european-air-quality-
105 database-8#tab-figures-produced; available years: 1973–2012) (Schultz et al., 2017). After
106 applying the same data selection criteria above, we get a total of 685 sites (289 for urban, 150 for
107 suburban and 246 for rural).

108 We calculated the linear trends for the European surface ozone at individual hours, and mean
109 values for daytime (local time: 07:00–19:00), nighttime (local time: 19:00–07:00) and full days
110 (24 h). For each daytime or nighttime period, the missing data varies between 6.8 and 34.6%

(Table 1). The monthly 5th, 50th and 95th percentile ozone concentrations for each period (per hour, daytime, nighttime and diurnal) are derived from the lowest, middle and highest 5th percentile hourly ozone mixing ratios of the corresponding period at individual stations in each month. Averaging over the 93 sites, we then also calculate the trends of different percentile ozone concentrations over the whole Europe.

To calculate the ozone trends per hour, during daytime, nighttime and per day, we then use the following statistical trend model (Weatherhead et al., 1998; Yoon and Pozzer, 2014):

$$Y_t = \mu + S_t + \omega X_t + N_t$$

Where Y_t denotes the monthly time series of ozone, μ is a constant term representing the offset, $X_t = t/12$ (with t as month) the number of years in the timeseries, and ω is the magnitude of the trend per year. S_t is a seasonal component in the trend estimates. N_t is the residual term of the interpolation. As the seasonal component does not have much impact on the statistical properties of the estimates of the other terms in the model, we use the deseasonalized monthly data to perform the trend analysis with a model of the form:

$$Y_t = \mu + \omega X_t + N_t$$

Using this formulation the linear trends are also analyzed separately for the observed monthly, seasonal and annual surface ozone concentration.

The standard deviation of ozone trends over the European stations is calculated with:

$$\sigma = \sqrt{\frac{1}{N}\sum_{i=1}^{N}(\omega_i - \alpha)^2}$$

where N is the total number of sites, ω_i is ozone trend at individual sites and α represents the average ozone trend.

2.2 ERA-Interim 2-meter temperature data

To help investigate the underlying effects of climate variability on ozone variations and trends, we relate the monthly variability of ozone to 2-meter temperature relevant to the European ground-level meteorology. The 2-meter temperature data is from the reanalysis product ERA-Interim, provided by the European Centre for Medium Range Weather Forecast (ECMWF) Public Datasets web interface (http://apps.ecmwf.int/datasets/), covering the data-rich period from 1979 and continuing in real time (Dee et al., 2011). Compared to the ERA-40, the ERA-Interim has an improved representation of the hydrological cycle, and stratospheric circulation (Dee and Uppala, 2009; Dee et al., 2011). The ERA-Interim atmospheric model and reanalysis system uses cycle 31r2 of ECMWF's Integrated Forecast System (IFS), configured for 60 vertical levels up to 0.1 hPa. The horizontal-spatial resolution is either in a full T255 spectral resolution or in the corresponding N128 reduced Gaussian grid (Dee et al., 2011). ERA-Interim assimilates

four analyses per day, at 00, 06, 12 and 18 UTC. ECMWF public website provides a large variety of data in uniform lat/long grids varying from 0.125° to 3°. Out of those, here, we analyze the monthly mean 2-meter temperature data which are archived on the 0.75° latitude by 0.75° longitude grid. Additional information (e.g. on current data availability) is available on the ECMWF website at http://www.ecmwf.int/research/era.

2.3 Atmospheric chemistry modeling

The ECHAM5/MESSy Atmospheric Chemistry (EMAC) model has been used to simulate surface ozone for the 1995–2014 periods. The EMAC model applies the second version of the Modular Earth Submodel System (MESSy2) to link multi-institutional computer codes (Jockel et al., 2016). The core atmospheric model is the 5th generation European Centre Hamburg general circulation model (ECHAM5) (Roeckner et al., 2006). EMAC simulated gas-phase tracers as well as aerosols have been extensively evaluated in previous studies (e. g. Pozzer et al., 2007; Pozzer et al., 2012).

In this work, we use the archived RC1SD-base-10a simulation results from the EMAC model conducted by the ESCiMo project (Jockel et al., 2016). The model results were simulated with version 5.3.02 for ECHAM5 and version 2.51 for MESSy. The archived data were obtained with a T42L90MA spatial resolution, i.e., with a T42 spherical representation which is corresponding to a quadratic Gaussian grid with approximately 2.8 latitude by 2.8 longitude, and 90 levels in the vertical, with the top level up to 0.01 hPa. To reproduce the observed meteorology, the method of Newtonian relaxation towards ERA-Interim reanalysis data (Dee et al., 2011) is applied to weakly nudge the dynamics of the general circulation model. Differently from the work of Jöckel et al. (2016), the model was re-run to cover the full period of measurements and also with a 1-hourly temporal resolution for ozone, in order to compare model results with hourly observational data. We also conducted a sensitivity simulation in which the anthropogenic emissions were kept constant (at the 1994 levels), to represent a scenario with fixed emissions throughout the years where observations are available to investigate the effects of emissions on ozone trends.

The chemical mechanism in the simulations considers the basic gas-phase chemistry of ozone, odd nitrogen, methane, alkanes, alkenes and halogens (bromine and chlorine). Here we use the Mainz Isoprene Mechanism (version 1; MIM1) to account for the chemistry of isoprene and additional non-methane hydrocarbons (NMHCs). This mechanism in total includes 310 reactions of 155 species and is included in the submodel MECCA (Jöckel et al., 2010; R. Sander et al., 2011).

Anthropogenic and biomass burning emissions in the model are incorporated as prescribed sources following the Chemistry-Climate Model Initiative (CCMI) recommendations (Eyring et al., 2013), using the MACCity (Monitoring Atmospheric Composition & Climate/City Zero Energy) emission inventory, which includes a seasonal cycle (monthly resolved) for biomass

181 burning (Diehl et al. 2012) and anthropogenic emissions (Granier et al. 2011). Additionally, the
182 emissions are vertically distributed as described by Pozzer et al. (2009). Since the total NMVOCs
183 (non-methane volatile organic compounds) values for anthropogenic sectors are not provided by
184 the MACCity raw dataset, they are recalculated from the corresponding species (Jockel et al.,
185 2016).

186 Emissions from natural sources have been prescribed as well, either as monthly resolved or
187 annually constant climatology. The spatial and temporal distributions of biogenic NMHCs are
188 based on Global Emissions InitiAtive (GEIA). In addition, the emissions of terrestrial dimethyl
189 sulfide (DMS), volcanic SO_2, halocarbons and ammonia are prescribed mostly based on
190 climatologies. The ocean-to-atmosphere fluxes of DMS, C_5H_8, and methanol are calculated by
191 the AIRSEA submodel (Pozzer et al., 2006) following the two-layer model by Liss and Slater
192 (1974). The emissions of soil NO_x (Yienger and Levy, 1995;Ganzeveld et al., 2002) and biogenic
193 isoprene (C_5H_8) (Guenther et al., 1995;Ganzeveld et al., 2002) are calculated online using the
194 submodel ONEMIS. The lightning NO_x emissions are calculated with the submodel LNOX (Tost
195 et al., 2007) following the parameterization by Grewe et al. (2001). This scheme links the flash
196 frequency to the thunderstorm cloud updraft velocity. Aerosols are included in the simulation,
197 although their heating rates and surface areas (needed for heterogeneous reactions) are prescribed
198 from an external climatology rather than interactive chemistry. Further details of the model setup
199 on the emissions, physical and chemical processes as well as the model evaluation with
200 observations can be found in Jöckel et al. (2016).

201 **3. Results**

202 **3.1 Ozone trends in EMEP and Airbase measurements**

203 Annual and seasonal mean daytime and nighttime ozone mixing ratios averaged over the EMEP
204 sites and Airbase sites are shown in Fig. 2. Ozone mixing ratios are maximum over the spring-to-
205 summer season and minimum over the fall-to-winter season for different type of station
206 classification. For annual mean ozone, the concentrations both in daytime and at night over rural
207 sites (EMEP sites and Airbase rural sites) are higher than those averaged over the Airbase
208 suburban and urban sites. Although the EMEP (93 sites) ozone and Airbase rural (246 sites)
209 ozone are calculated based on different number of sites, the ozone trends (shown in each panel in
210 Fig. 2) for annual and seasonal means are similar both during daytime and at night. For the
211 Airbase suburban and urban sites, ozone has increased rapidly with the statistically significant
212 growth rates of 0.09–0.83 µg/m^3/y, except that a decline rate of -0.19 µg/m^3/y (P-value < 0.01) is
213 also visible for suburban summer ozone during 1995–2012. These suburban and urban ozone
214 enhancements (0.20–0.59 µg/m^3/y for annual means; P-value < 0.01) are contrast to the slight
215 rural ozone decrease (-0.09 – -0.02 µg/m^3/y for annual means; with an increasing trend for winter
216 ozone and a decreasing trend for summer ozone). Similar results of the differences in trend
217 between rural and urban/suburban sites have been shown by recent study (chang et al., 2017). As
218 the EMAC model version used here is on a coarse resolution, which is not suitable to investigate

the observed contrast ozone trends among the urban, suburban and rural stations, we focus on the analysis of ozone levels and changes over the regional background areas monitored by EMEP network in the following results.

Fig. 3 shows the trends in ozone concentrations (monthly mean, 5th, 50th and 95th percentile) over EMEP sites during the 1995–2014 period, for each hour of the day. While the average ozone concentrations (and 50th percentiles) do not show significant trends, the 5th and 95th percentile ozone show significant trends with a clear diel cycle. The 95th percentile ozone shows a decreasing trend over Europe during the 1995–2014 period with the trend being most pronounced (-0.9 ± 0.5 μg/m^3/y; P-value < 0.01) during midday (1100-1500 h). 95th percentile ozone concentrations also show a decreasing trend during the night, however the trends are observed to be smaller (-0.5 ± 0.35 μg/m^3/y; P-value < 0.01). For the ozone trend of 95th percentile at individual station, 84 sites (90%) are characterized by decreasing trend in daytime and 78 sites (84%) at night (Fig. 5 and Fig. S2). Here the standard deviation depicts the variability of the trends among the stations, and therefore reflects the almost homogeneous decrease over entire Europe. Interestingly, in contrast with the 95th percentile, the 5th percentile ozone over Europe shows an increasing trend especially during midday (0.3 ± 0.16 μg/m^3/y; P-value < 0.01). Further, the temporal evolutions of ozone anomalies during the 1995–2014 period are shown for 5th and 95th percentile in Fig. S1. The 95th percentile ozone trend indicates a general decline in the photochemical buildup of ozone during noon hours, with the exception of strongly enhanced ozone during 2003. The inter-annual variability is observed to be very large with ozone anomalies in excess of 35 μg/m^3 in 2003 relative to 2014. For 95th percentile ozone, the sharp increase by up to 20 μg/m^3 in the year 2003 occurred during a strong European heat wave (Section 4.2). The analysis of individual year observations here shows that the increasing trend in the 5th percentile ozone is a robust feature with most of the recent years showing stronger noontime build up in ozone as compared to the 1990s. During the study period the variability in noontime ozone anomalies is however lower (~10 μg/m^3) in the 5th percentile ozone compared to the 95th percentile ozone.

Consistently with the results obtained for hourly ozone, when the observational data is reduced to diurnal values, a growth rate of 0.22 ± 0.15 μg/m^3/y (P-value < 0.01) is calculated for the European mean 5th percentile ozone, while a stronger decline rate of -0.57 ± 0.34 μg/m^3/y (P-value < 0.01) is estimated for the European mean 95th percentile ozone (see Table 2). Hereafter we will mainly focus on trends in the daytime mean, nighttime mean, 5th percentile and 95th percentile ozone concentrations.

The observed long-term reduction in 95th percentile ozone concentrations over Europe concurs with the reduction in anthropogenic emissions of ozone precursors (Fig. S6). Anthropogenic emissions of NO_x and CO over Europe declined by 35% and 58%, respectively, as calculated from the MACCity inventory. Slower rates of ozone reduction during nighttime are suggested to be combined effects of reduced titration due to lower NOx emissions, and an increase in the

global background ozone concentrations during this period, probably due to growing precursor emissions worldwide since 1995, which has been predicted by Lelieveld and Dentener (2000) based on atmospheric chemistry – transport modeling, and corroborated by satellite observations (Richter et al., 2005; Krotkov et al., 2016). The effect of anthropogenic emissions is discussed in more detail in the Section 4.1.

Fig. 4 further shows ozone trends for each month of the year. The slight growth rates in the 5th percentile ozone are approximately equally distributed at the level of 0.1 ± 0.12 µg/m^3/y (P-value > 0.05), probably due to the absence of ozone diurnal cycle, affected by NO_x anthropogenic emissions, for 5th percentile especially in winter. Conversely, the monthly trends for the 95th percentile ozone are negative with a most rapid decrease rate of -1.67 ± 0.4 µg/m^3/y (P-value < 0.01) in August. For the 50th percentiles (mean) the seasonal cycle of ozone trends decline unevenly from January to August, then pick up in the following months. It leads to the fastest ozone growth in December when the ozone production is minor due to the relatively lowest solar UV fluxes and temperatures, and the maximum ozone decline in August, which is the photochemically most active month in Europe. In December, the 50th (mean) percentile ozone increases at a rate of 0.41 ± 0.21 µg/m^3/y (0.32 ± 0.09 µg/m^3/y), while a decline rate of -0.40 ± 0.24 µg/m^3/y (-0.51 ± 0.13 µg/m^3/y) is calculated in August.

Table 3 shows the trends in European mean (averaged over the 93 sites) seasonal ozone concentrations analyzed separately for day- and nighttime. The ozone concentrations show pronounced differences in trends over the different seasons. The mean surface ozone in summer, averaged over the selected 93 sites, declines at rates of -0.32 ± 0.24 µg/m^3/y and -0.20 ± 0.27 µg/m^3/y during day- and nighttime, respectively. It is mainly related to the rapid decline in the highest levels (95th percentile) of ozone with rates of -1.10 ± 0.61 µg/m^3/y (daytime) and -0.71 ± 0.52 µg/m^3/y (nighttime). Although the 95th percentile ozone in spring declines almost as fast as during summer, the decrease in spring for the 95th percentile ozone is compensated by the growth in 5th percentile ozone, leading to much lower decrease rates in spring compared to summer for the mean ozone concentrations. Finally, in winter ozone grows at a rate of ~0.10 µg/m^3/y. This increase occurs mostly in the lower level (5th percentile) ozone concentrations, with growth rates of 0.25 ± 0.15 µg/m^3/y (daytime) and 0.14 ± 0.22 µg/m^3/y (nighttime).

For the trends in annual mean ozone mixing ratios, a decline in the 95th percentile ozone (daytime: -0.81± 0.46 µg/m^3/y; nighttime: -0.57 ± 0.36 µg/m^3/y) is observed while an increase in the 5th percentile ozone (0.22 ± 0.17 and 0.16 ± 0.17 µg/m^3/y for day- and nighttime, respectively, is calculated, resulting in statistically not-significant decreasing trends (daytime: -0.09 ± 0.24; nighttime: -0.05 ± 0.23 µg/m^3/y) (Table 3).

Fig. 5 further shows the ozone trends distribution site-by-site over the 93 selected stations for daytime mean, 5th and 95th percentile ozone during the four seasons. The 95th percentile ozone trend shows a decline at most of the selected sites, although ozone increases are also visible at

several sites, especially in fall-to-winter. The annual ozone trend averaged over all sites during daytime (-0.62 μg/m^3/y) is nearly twice that during nighttime (-0.35 μg/m^3/y, Fig. S2). For the 5th percentile ozone, the annual means have grown over the western and central European sites, in contrast with declines in ozone at other locations over the northern and southern Europe. These geographical differences in ozone trends are probably explained by the effects of a general decrease in European anthropogenic precursor emissions, being partly offset by those of climate variability (see Sect. 4.2 for discussion of Fig. 11 and Fig. S10). Averaged across all sites, the 5th percentile ozone has slightly grown during day- as well as nighttime. The geographical differences in ozone trends are most significant in spring with an average growth rate of 0.01 μg/m^3/y (Fig. 5). The ozone trends spatial distribution in the daytime (Fig. 5) much resembles that of the ozone trends in nighttime (Fig. S2) for the mean, 5th percentile as well as 95th percentile ozone.

3.2 Ozone exceedance trends

Based on the European directive for ozone concentrations limits, we calculate the number of exceedances for the information threshold and long-term objective (Fig. 6). Averaged over the selected 93 sites, the exceedances of the information threshold as well as the long-term objective have declined at rates of -3.2% and -2.5% per year relative to 1995. The decrease accelerated after the year 2003, during which a European heat wave raised summer temperatures by 20 to 30% (in degrees Celsius) compared to the seasonal average over a large part of the continent, extending from northern Spain to the Czech Republic and from Germany to Italy. The variations in the exceedances are inter-annually consistent with the changes in the annual 95th percentile ozone, with a significant correlation coefficient of 0.93 for information threshold exceedances and 0.90 for long-term objective exceedances.

3.3 Ozone trends from EMAC simulation

The same analysis performed on the observations has been carried out on the EMAC model results, i.e., for the same period covered by the observations. To ensure spatiotemporal consistency with the EMEP data, modeled ozone concentrations are sampled at the times and locations of the measurements.

Fig. 7 compares the time series of modeled and observed monthly mean ozone over Europe. Although the model overestimates the measurements with a mean bias of 4.3 μg/m^3 over the 1995–2014 period, the simulation results are highly correlated with observed ozone, with a significant correlation coefficient of 0.91. The high bias may be explained by the coarse grid resolution of 2.8 degrees that was applied, leading to the artificial dispersion of localized NO_x emissions, which optimizes NO_x concentrations over Europe with respect to chemical O_3 formation, also noticed by Joeckel et al (2016). Such overestimation of the observed ozone due to coarse model horizontal resolution has been reported by Lin et al. (2008) and Yan et al. (2014,

2016). The overestimation after 2010 becomes more evident (mean bias 5.4 μg/m^3), mostly due to the emissions used in the model version used, being prescribed up to the year 2005 and predicted in the subsequent period. The modeled ozone biases are slightly higher (mean bias: 5.2 μg/m^3 and 6.7 μg/m^3 for 1995–2014 and 2010–2014, respectively) compared to the observed de-seasonalized time series. Nevertheless, EMAC model can reproduce the observed inter-annual and seasonal variability of ozone, with statistically significant correlation coefficients at most observation sites. For the diurnal, daytime as well as nighttime mean ozone averaged across the 93 sites, the model-observation correlation is 0.84–0.92 (0.62–0.70 for de-seasonalized time series).

Fig. 1 also shows the spatial distribution of observed and modeled mean ozone mixing ratios, as well as the modeled biases for every five years during 1995-2014 over the selected 93 sites. It is shown that for most monitoring stations the model overestimates the observed background ozone concentrations with the bias up to 15 μg/m^3. Ozone overestimation has been observed also in other EMAC simulations when compared to satellite data (Jöckel et al., 2016). Relatively frequent overestimations (> 10 μg/m^3) occur over the coastal and marine sites where the coarse model resolution mixes the polluted air over land with cleaner air masses. Underestimation of modeled ozone also occurs over several sites located at the central Europe. These simulated ozone underestimations are probably due to the underestimation of precursor emissions (especially NO_x) discussed by Oikonomakis et al. (2017).

The EMAC modeled ozone trends per hour are shown in Fig. 7. The agreement with the observationally estimated trends is good, although the model tends to overestimate the trends by 0.12 μg/m^3/y, 0.23 μg/m^3/y, 0.08 μg/m^3/y, and 0.36 μg/m^3/y for the mean, 5th, 50th and 95th percentile ozone, respectively. The higher ozone overestimation since 2010 may be the dominant reason for the trend overestimation especially for 95th percentile. The measured diurnal cycle of the ozone trends (Fig. 3) is well captured by the EMAC model for the 5th and 95th percentile ozone concentrations. Consistently, the modeled temporal evolutions (Fig. S3) of annual European 5th percentile ozone anomalies are larger compared to the observations (~15 μg/m^3 versus ~10 μg/m^3 enhancements during photochemical buildup of ozone at midday hours during 1990–2014), while being smaller for the 95th percentile (~21 μg/m^3 versus ~30 μg/m^3). Further, the EMAC model reproduces the jump in high level ozone concentrations during the year 2003 that was affected by a major heat wave.

For the diurnal mean values, averaged over Europe, the model produces higher growth rates for the 5th percentile ozone and weaker decrease rates for the 95th percentile ozone compared to the observed trends (Table 2). For the 50th percentile and mean ozone trends averaged over Europe, the model shows statistically insignificant changes, similar to the observed trends (Table 2). Fig. S4 further shows the spatial distribution of the simulated diurnal ozone trends. It corroborates that central Europe experiences the highest growth rate for the averaged (also 50th percentile) and 5th percentile ozone concentrations, and the strongest reduction for the 95th percentile ozone during all seasons.

369 For the trends per month, the EMAC model reproduces the observed variability with statistically
370 significant correlation coefficients of 0.88–0.90 for the mean, 50th and 95th percentile ozone
371 trends (Fig. 4 and Fig. S5). Seasonally, for the 95th percentile ozone the modeled ozone trends are
372 much weaker than from measurements in all seasons except the autumn (Table 3). The decreased
373 higher level ozone is probably driven by the anthropogenic ozone precursor emission decline
374 over these years, which has been studied in previous work of ozone change drivers and
375 corroborated in Sect. 4.1 with a sensitivity simulation. For the 5th percentile ozone, especially for
376 the daytime period, the increasing trends are enhanced in the model results during all seasons
377 (Table 3). The possible reason for these simulated enhanced ozone trends is the overestimation of
378 the decline of European anthropogenic ozone precursor emissions (decreasing more rapidly than
379 observed) in EMAC.

380 **4. Anthropogenic emissions and climate variability**

381 **4.1 Effects of anthropogenic emissions**

382 A sensitivity simulation is conducted with constant global anthropogenic emissions to test the
383 sensitivity of observed European background ozone to inter-annual variability in climate, by
384 removing the effects of anthropogenic emission changes. Consequently, the decline in European
385 emissions (Fig. S6) is removed from the EMAC model. With constant emissions, the modeled
386 ozone shows a slight increase at the midday hours for the 95th percentile and a slight decrease for
387 the 5th percentile, in contrast to the trends calculated from the control simulation. In the
388 sensitivity simulations no significant trend (less than 0.1 $\mu g/m^3/y$) for any hour of the day is
389 found, and also no contrast in ozone trends between the 5th and 95th percentiles (Fig. 8), which
390 was well reproduced by the control simulation. Therefore, it appears that both the decreases in
391 95th percentile ozone and the enhancements in 5th percentile ozone are associated with the rapid
392 decline in the precursor gases anthropogenic emissions over Europe, notably of NO_x, prescribed
393 by the MACCity inventory (Fig. S6). These results reflect the effectiveness in controlling high-
394 level ozone, but being unsuccessful in controlling the lower level ozone. Evidently, the 35%
395 reduction in NO_x emissions in Europe was not sufficient to achieve substantial reductions in
396 ozone, especially of background levels, which are affected by growing emissions in Asia that are
397 transported hemispherically (Lelieveld and Dentener, 2000; Lawrence and Lelieveld, 2010).

398 Averaging over the selected 93 sites, we calculate the number of exceedances for the information
399 threshold both in the control and the sensitivity simulation (Fig. 9). In the control simulation, the
400 exceedances of the information threshold have declined at rates of -2.5% per year relative to
401 1995, slightly smaller than the observed decrease rate of -3.2%. The variations in exceedances are
402 inter-annually consistent with the observations, with a significant correlation coefficient of 0.61.
403 However, in the sensitivity simulation, the decline rate (-0.6%) in the exceedances is much
404 smaller than the rates in the control simulation and in the observations.

By fixing the anthropogenic emissions, ozone trends in each month for the 95th percentile ozone show no obvious decline but rather a slight enhancement with growth rates of -0.23 – 0.50 $\mu g/m^3/y$. For the 5th percentile ozone and compared to the control simulation, there is no increase but a slight decrease at a rate of -0.51 – 0.15 $\mu g/m^3/y$ in months of the year (Fig. S7). For the trends in annual mean ozone mixing ratios simulated in the sensitivity simulation, an enhancement in the 95th percentile ozone (daytime: 0.16 ± 0.18 $\mu g/m^3/y$; nighttime: 0.10 ± 0.15 $\mu g/m^3/y$) is calculated while a decline in the 5th percentile ozone (-0.11 ± 0.14 and -0.07 ± 0.12 $\mu g/m^3/y$ for daytime and nighttime, respectively) is estimated, contrasting to but smaller in the absolute value than the trends in the control simulation. This contrast has been also shown in the trends for individual hour of the day between control and sensitivity simulations (Fig. 8). These results show that the effects of decline in anthropogenic emissions on European background ozone change are somewhat offset by the impacts of climate variability. This compensation effect is not only for the high level ozone concentrations, which has been reported by previous studies (Lin et al., 2017), but also for the low level ozone concentrations.

4.2 Effects of climate variability

4.2.1 Heat wave effects

As discussed in number of studies (e.g., Filleul et al, 2006, Vautard et al, 2005, Garcia-Herrera et a 2010, Vieno et al 2010), the 2003 heat waves caused favorable meteorology for ozone buildup, leading to very high ozone concentrations during the summer period (from July to August). Especially, in August 2003, coinciding with a major heat wave in central and northern Europe, massive forest fires were observed from the Terra and MODIS satellite in many parts of Europe, particularly in the south and most pronounced in Portugal and Spain (Pace et al., 2005; Hodzic et al., 2006, 2007; Solberg et al., 2008). Long-range transport of fire emissions have been found to give rise to significantly elevated air pollution concentration and proved to be contributed to the European ozone peak values in August 2003 (Solberg et al., 2008; Tressol et al., 2008; Ordóñez et al., 2010).

Fig. 10 shows the distribution of the difference in the exceedances between 2003 and averaged over 1995-2002 for the information threshold as well as the long-term objective over individual site. Except for some northern sites, the exceedances in 2003 are much more frequent than the average from 1995 to 2002 over most of the observational sites, especially over central Europe. This exceedance anomaly distribution in 2003 relative to the period of 1995-2002 coincides with the 2-meter temperature anomaly distribution, with a statistically significant correlation up to 0.64 (P-value < 0.01 under a *T*-test; Fig. S8).

4.2.2 Effects of inter-annual climate variability

439 The exceedance anomaly of information threshold and long-term objective during the year 2003
440 with respect to the 1995-2002 period follows the anomaly in ozone concentrations, in turn
441 consistent with the temperature anomaly. Fig. 11 shows the correlations between the monthly
442 mean 2-meter temperature and the monthly mean, 5th and 95th percentile ozone for diurnal,
443 daytime and nighttime concentrations. Most of these site-by-site correlations are statistically
444 significant (P-value < 0.05 under a *T*-test; shown as triangles in Fig. 11) with high fraction (66%–
445 91%) of sites for which significant correlation exist. For each metric (mean and percentiles for
446 diurnal, daytime and nighttime), it corroborates the high correlations over central Europe with
447 statistically significant values up to ~0.82 (P-value < 0.01). It indicates that the surface ozone
448 mixing ratios are highly sensitive to enhanced air temperature, being favorable for photochemical
449 O_3 production, which has been reported by previous studies (Lin et al., 2017; Yan et al., 2018 and
450 references therein). For different seasons, ozone variations in fall are most closely affected by
451 temperature (Fig. S9), followed by the spring and summer ozone. The weakest linkage between
452 ozone and temperature is in winter with few sites for which significant correlation exist
453 especially for 95th percentile.

454 In contrast to the positive correlations over central and southern stations, ozone concentrations
455 over the northern and western sites are negative and significantly correlated with temperature,
456 associated with statistically insignificant correlations at several sites located in the transition
457 regions from positive-correlation to negative-correlation (Fig. 11). This may be related to the
458 influence of the Northern Atlantic Oscillation (NAO; a dominant mode of winter climate
459 variability in the North Atlantic region including Europe; higher correlations with ozone in winter
460 shown in Fig. S11), which had an opposite impact on ozone over northern and western compared
461 to central and southern Europe (Fig. S10). This is because the positive NAO phase is associated
462 with enhanced pressure gradient between subtropical high pressure center (stronger than usual)
463 and Icelandic low (deeper than normal). It can result in more and stronger winter storms crossing
464 the Atlantic Ocean on a more northerly pathway, and consequently lead to warm and wet air in
465 northern Europe. Compared to the impact of temperature, the effect of NAO on ozone are
466 relatively modest with much lower correlations (Fig. 11 and Fig. S10). The correlations of less
467 than 30% of the sites pass the significance test (P-value < 0.05). These results underscore that the
468 large-scale climate variability affects the inter-annual variability of European background ozone.

469 In the simulation with constant emissions, however, the modeled ozone fluctuation of annual
470 European ozone anomalies for individual hours is comparable in magnitude with the results in the
471 control simulation (Fig. S7). In both simulations, the fluctuation dominates around midday for 5th
472 (~15 µg/m^3 in the base simulation versus ~13 µg/m^3 in sensitivity simulation) and 95th (~21
473 µg/m^3 versus ~20 µg/m^3) percentile ozone (Fig. S7 and Fig. S3). In addition, the variations in the
474 exceedances of the information threshold are inter-annually consistent with the observations and
475 the control simulation, with significant correlation coefficients of 0.54 and 0.56, respectively,
476 comparable to the correlations between observations and control simulation (Fig. 9). Further
477 correlations between the European averaged monthly mean 2-meter temperature and the modeled

478 monthly mean (50th), 5th and 95th percentile ozone in the sensitivity simulation are statistically
479 significant with correlation coefficients of 0.69–0.78 for diurnal, day- and nighttime
480 concentrations, consistent with the correlations (0.70–0.81) between 2-meter temperature and
481 simulated European ozone in the control simulation. These results clearly show that the
482 interannual ozone variations are affected by climate variability.

483 **5. Conclusions and outlook**

484 Based on EMEP observed background ozone in the period 1995–2014, we analyzed the annual
485 and seasonal trends of the mean, the 5th, 50th and 95th percentile of the ozone concentrations at
486 different temporal distributions, i.e., hourly, diurnal, day- and nighttime. Results show that
487 although reductions in anthropogenic emissions have lowered the peak ozone concentrations
488 (sites with statistically significant trends: 91 out of 93 sites; 98%), especially during daytime in
489 the period 1995–2014, the lower level ozone concentrations have increased (sites with
490 statistically significant trends: 71 out of 93 sites; 76%) continually since 1995 over Europe. This
491 leads to insignificant trends in the 50th percentile and mean ozone. Both the 5th and 95th percentile
492 ozone trends follow a diel cycle with largest trends during periods of strong photochemical
493 activity. These contrasting ozone trends per hour during the day and at different concentration
494 levels are well reproduced by the EMAC chemistry-climate model, although the model slightly
495 overestimates observed ozone at the surface. Furthermore, the numbers of exceedances of the
496 information threshold and long-term objective have continuously declined during the 20-year
497 period considered, and the decrease has accelerated since the year 2003.

498 Sensitivity simulations with constant emissions in the EMAC model, and correlation analysis
499 between modeled ozone and the ERA-Interim 2-meter temperature help distinguish effects of
500 climate and anthropogenic emissions on ozone variations and trends. Climate variability
501 generally regulates the interannual variations of European surface ozone, while the changes in
502 anthropogenic emissions predominantly contribute to ozone trends. However, it appears that the
503 negative ozone trend due to European emission controls has been counteracted by a climate
504 related tendency as well as hemispheric dispersion of pollutants from other regions. We note that
505 our analysis over 1995–2014 is a timeframe too short for the analysis of climate tendencies
506 (formally a 30-year period is necessary). Thus, here the climate related variability is mainly
507 driven by the large-scale processes like NAO and heat wave occurrence, which may be
508 influenced by climate change.

509 In contrast to the observed diverse trends of European background ozone, significant ozone
510 enhancements are found for the annual means (0.20–0.59 µg/m^3/y) as well as seasonal means
511 (0.09–0.83 µg/m^3/y), both during daytime and at night over the suburban and urban stations
512 during 1995–2012 based on the Airbase sites. These increasing trends are interesting and should
513 be investigated further in view of the continuous decline in European anthropogenic emissions.

514 **Acknowledgements**

References

519 Bloomer, B. J., Stehr, J. W., Piety, C. A., Salawitch, R. J., and Dickerson, R. R.: Observed relationships of ozone air
520   pollution with temperature and emissions, Geophysical Research Letters, 36, L09803,
521   10.1029/2009gl037308, 2009.
522 Brown-Steiner, B., Hess, P. G., and Lin, M. Y.: On the capabilities and limitations of GCCM simulations of
523   summertime regional air quality: A diagnostic analysis of ozone and temperature simulations in the US
524   using CESM CAM-Chem, Atmospheric Environment, 101, 134-148, 10.1016/j.atmosenv.2014.11.001,
525   2015.
526 Chang K-L, Petropavlovskikh I, Cooper OR, Schultz MG, Wang T.: Regional trend analysis of surface ozone
527   observations from monitoring networks in eastern North America, Europe and East Asia, Elem Sci Anth, 5,
528   50-71, DOI: http://doi.org/10.1525/elementa.243, 2017.
529 Coates, J., Mar, K. A., Ojha, N., and Butler, T. M.: The influence of temperature on ozone production under varying
530   NO_x conditions – a modelling study, Atmos. Chem. Phys., 16, 11601-11615, https://doi.org/10.5194/acp-16-
531   11601-2016, 2016.
532 Colette, A., Granier, C., Hodnebrog, O., Jakobs, H., Maurizi, A., Nyiri, A., Bessagnet, B., D'Angiola, A., D'Isidoro,
533   M., Gauss, M., Meleux, F., Memmesheimer, M., Mieville, A., Rouil, L., Russo, F., Solberg, S., Stordal, F.,
534   and Tampieri, F.: Air quality trends in Europe over the past decade: a first multi- model assessment,
535   Atmospheric Chemistry and Physics, 11, 11657-11678, 10.5194/acp-11-11657-2011, 2011.
536 Cooper, O. R., Gao, R.-S., Tarasick, D., Leblanc, T., and Sweeney, C.: Long-term ozone trends at rural ozone
537   monitoring sites across the United States, 1990-2010, Journal of Geophysical Research-Atmospheres, 117,
538   10.1029/2012jd018261, 2012.
539 Dee, D. P., Uppala, S. M., Simmons, A. J., Berrisford, P., Poli, P., Kobayashi, S., Andrae, U., Balmaseda, M. A.,
540   Balsamo, G., Bauer, P., Bechtold, P., Beljaars, A. C. M., van de Berg, L., Bidlot, J., Bormann, N., Delsol,
541   C., Dragani, R., Fuentes, M., Geer, A. J., Haimberger, L., Healy, S. B., Hersbach, H., Holm, E. V., Isaksen,
542   L., Kallberg, P., Koehler, M., Matricardi, M., McNally, A. P., Monge-Sanz, B. M., Morcrette, J. J., Park, B.
543   K., Peubey, C., de Rosnay, P., Tavolato, C., Thepaut, J. N., and Vitart, F.: The ERA-Interim reanalysis:
544   configuration and performance of the data assimilation system, Quarterly Journal of the Royal
545   Meteorological Society, 137, 553-597, 10.1002/qj.828, 2011.
546 Dee, D. P., and Uppala, S.: Variational bias correction of satellite radiance data in the ERA-Interim reanalysis,
547   Quarterly Journal of the Royal Meteorological Society, 135, 1830-1841, 10.1002/qj.493, 2009.
548 Diehl, T., Heil, A., Chin, M., Pan, X., Streets, D., Schultz, M., and Kinne, S.: Anthropogenic, biomass burning, and
549   volcanic emissions of black carbon, organic carbon, and SO2 from 1980 to 2010 for hindcast model
550   experiments, Atmos. Chem. Phys. Discuss., https://doi.org/10.5194/acpd-12-24895-2012, 2012.
551 Eyring, V., Lamarque, J.-F., Hess, P., Arfeuille, F., Bowman, K., Chipperfield, M., Duncan, B., Fiore, A., Gettelman,
552   A., Giorgetta, M., Granier, C., Hegglin, M., Kinnison, D., Kunze, M., Langematz, U., Luo, B., Martin, R.,
553   Matthes, K., Newman, P., Peter, T., Robock, A., Ryerson, A., Saiz-Lopez, A., Salawitch, R., Schultz, M.,
554   Shepherd, T., Shindell, D., Stähelin, J., Tegtmeier, S., Thomason, L., Tilmes, S., Vernier, J.-P., Waugh, D.,
555   and Young, P.: Overview of IGAC/SPARC Chemistry-Climate Model Initiative (CCMI) Community
556   Simulations in Support of Upcoming Ozone and Climate Assessments, available at: http://www.sparc-
557   climate.org/fileadmin/customer/6_Publications/Newsletter_PDF/40_SPARCnewsletter_Jan2013_web.pdf,
558   2013.

EEA, 2013 EEA, Exposure of Ecosystems to Acidification, Eutrophication and Ozone (Indicator CSI 005), (2013) http://www.eea.europa.eu/data-and-maps/indicators/exposure-of-ecosystems-to-acidification-2/exposure-of-ecosystems-to-acidification-5

Fu, T.-M., Zheng, Y., Paulot, F., Mao, J., and Yantosca, R. M.: Positive but variable sensitivity of August surface ozone to large-scale warming in the southeast United States, Nature Climate Change, 5, 454-458, 10.1038/nclimate2567, 2015.

Ganzeveld, L. N., Lelieveld, J., Dentener, F. J., Krol, M. C., Bouwman, A. J., and Roelofs, G. J.: Global soil-biogenic NOx emissions and the role of canopy processes, Journal of Geophysical Research-Atmospheres, 107, 10.1029/2001jd001289, 2002.

Guenther, A., Hewitt, C. N., Erickson, D., Fall, R., Geron, C., Graedel, T., Harley, P., Klinger, L., Lerdau, M., McKay, W. A., Pierce, T., Scholes, B., Steinbrecher, R., Tallamraju, R., Taylor, J., and Zimmerman, P.: A GLOBAL-MODEL OF NATURAL VOLATILE ORGANIC-COMPOUND EMISSIONS, Journal of Geophysical Research-Atmospheres, 100, 8873-8892, 10.1029/94jd02950, 1995.

Guerreiro, C. B. B., Foltescu, V., and de Leeuw, F.: Air quality status and trends in Europe, Atmospheric Environment, 98, 376-384, 10.1016/j.atmosenv.2014.09.017, 2014.

Granier, C., Bessagnet, B., Bond, T., D'Angiola A., van der Gon H. D., Frost G. J., Heil A., Kaiser J. W., Kinne S., Klimont Z., Kloster S., Lamarque J. F., Liousse C., Masui T., Meleux F., Mieville A., Ohara T., Raut J. C., Riahi K., Schultz M. G., Smith S. J., Thompson A., Aardenne J., van der Werf G. R. and van Vuuren D. P.: Evolution of anthropogenic and biomass burning emissions of air pollutants at global and regional scales during the 1980–2010 period, Climatic Change, 109, 163-190, https://doi.org/10.1007/s10584-011-0154-1, 2011

Grewe, V., Brunner, D., Dameris, M., Grenfell, J., Hein, R., Shindell, D., and Staehelin, J.: Origin and variability of upper tropospheric nitrogen oxides and ozone at northern midlatitudes, Atmos. Environ., 35, 3421–3433, doi:10.1016/S1352-2310(01)00134-0, 2001.

Hjellbrekke, A-G., Solberg, S., 2002. Ozone measurments 2000. EMEP/CCC-Report 5/2002.

Hodzic, A., Vautard, R., Chepfer, H., Goloub, P., Menut, L., Chazette, P., Deuze, J.-L., Apituley, A., and Couvert, P.: Evolu-´ tion of aerosol optical thickness over Europe during the August 2003 heat wave as seen from CHIMERE model simulations and POLDER data, Atmos. Chem. Phys., 6, 1853–1864, 2006, http://www.atmos-chem-phys.net/6/1853/2006/.

Hodzic, A., Madronich, S., Bohn, B. Massie, S., Menut, L., and Wiedinmyer, C.: Wildfire particulate matter in Europe during summer 2003: meso-scale modeling of smoke emissions, transport and radiative effect., Atmos. Chem. Phys., 7, 4043–4064, 2007, http://www.atmos-chem-phys.net/7/4043/2007/.

Jacob, D. J., and Winner, D. A.: Effect of climate change on air quality, Atmospheric Environment, 43, 51-63, 10.1016/j.atmosenv.2008.09.051, 2009.

Jhun, I., Coull, B. A., Zanobetti, A., and Koutrakis, P.: The impact of nitrogen oxides concentration decreases on ozone trends in the USA, Air Quality, Atmosphere & Health, 1-10, 2014.

Jöckel, P., Kerkweg, A., Pozzer, A., Sander, R., Tost, H., Riede, H., Baumgaertner, A., Gromov, S., and Kern, B.: Development cycle 2 of the Modular Earth Submodel System (MESSy2), Geosci. Model Dev., 3, 717–752, doi:10.5194/gmd-3-717-2010, 2010.

Jockel, P., Tost, H., Pozzer, A., Kunze, M., Kirner, O., Brenninkmeijer, C. A. M., Brinkop, S., Cai, D. S., Dyroff, C., Eckstein, J., Frank, F., Garny, H., Gottschaldt, K. D., Graf, P., Grewe, V., Kerkweg, A., Kern, B., Matthes, S., Mertens, M., Meul, S., Neumaier, M., Nutzel, M., Oberlander-Hayn, S., Ruhnke, R., Runde, T., Sander, R., Scharffe, D., and Zahn, A.: Earth System Chemistry integrated Modelling (ESCiMo) with the Modular Earth Submodel System (MESSy) version 2.51, Geoscientific Model Development, 9, 1153-1200, 10.5194/gmd-9-1153-2016, 2016.

Jonson, J. E., Simpson, D., Fagerli, H., and Solberg, S.: Can we explain the trends in European ozone levels?, Atmos. Chem. Phys., 6, 51-66, https://doi.org/10.5194/acp-6-51-2006, 2006.

Krotkov, N. A., McLinden, C. A., Li, C., Lamsal, L. N., Celarier, E. A., Marchenko, S. V., Swartz, W. H., Bucsela, E. J., Joiner, J., Duncan, B. N., Boersma, K. F., Veefkind, J. P., Levelt, P. F., Fioletov, V. E., Dickerson, R.

608   R., He, H., Lu, Z., and Streets, D. G.: Aura OMI observations of regional SO2 and NO2 pollution changes
609   from 2005 to 2015, Atmos. Chem. Phys., 16, 4605-4629, https://doi.org/10.5194/acp-16-4605-2016, 2016.

610   Liss, P. and Slater, P.: Flux of Gases across the Air-Sea Interface, Nature, 247, 181–184, doi:10.1038/247181a0,
611   1974.

612   Langner, J., R. Bergström, and V. Foltescu: Impact of climate change on surface ozone and deposition of sulphur and
613   nitrogen in Europe, Atmospheric Environment, vol. 39, no. 6, pp. 1129–1141, 2005.

614   Langner, J., Engardt, M., Baklanov, A., Christensen, J. H., Gauss, M., Geels, C., Hedegaard, G. B., Nuterman, R.,
615   Simpson, D., Soares, J., Sofiev, M., Wind, P., and Zakey, A.: A multi-model study of impacts of climate
616   change on surface ozone in Europe, Atmos. Chem. Phys., 12, 10423-10440, https://doi.org/10.5194/acp-12-
617   10423-2012, 2012.

618   Lawrence, M. G. and Lelieveld, J.: Atmospheric pollutant outflow from southern Asia: a review, Atmos. Chem.
619   Phys., 10, 11017-11096, https://doi.org/10.5194/acp-10-11017-2010, 2010.

620   Lefohn, A. S., Shadwick, D., and Oltmans, S. J.: Characterizing changes in surface ozone levels in metropolitan and
621   rural areas in the United States for 1980-2008 and 1994-2008, Atmospheric Environment, 44, 5199-5210,
622   10.1016/j.atmosenv.2010.08.049, 2010.

623   Lelieveld, J., and Dentener, F.J.: What controls tropospheric ozone? J. Geophys. Res., 105, 3531-3551, 2000.

624   Lelieveld, J., Evans, J. S. Fnais, M., Giannadaki, D., and Pozzer, A.: The contribution of outdoor air pollution
625   sources to premature mortality on a global scale, Nature, 525, 367-371, 2015.

626   Lin, J. T., Youn, D., Liang, X. Z., and Wuebbles, D. J.: Global model simulation of summertime US ozone diurnal
627   cycle and its sensitivity to PBL mixing, spatial resolution, and emissions, Atmospheric Environment, 42,
628   8470-8483, 10.1016/j.atmosenv.2008.08.012, 2008.

629   Lin, M., Fiore, A. M., Horowitz, L. W., Langford, A. O., Oltmans, S. J., Tarasick, D., and Rieder, H. E.: Climate
630   variability modulates western US ozone air quality in spring via deep stratospheric intrusions, Nature
631   Communications, 6, 7105, 10.1038/ncomms8105, 2015.

632   Lin, M. Y., Horowitz, L. W., Payton, R., Fiore, A. M., and Tonnesen, G.: US surface ozone trends and extremes
633   from 1980 to 2014: quantifying the roles of rising Asian emissions, domestic controls, wildfires, and
634   climate, Atmospheric Chemistry and Physics, 17, 2943-2970, 10.5194/acp-17-2943-2017, 2017.

635   F. Meleux, F. Solmon, F. Giorgi: Increase in summer European ozone amounts due to climate change. Atmospheric
636   Environment, 41, pp. 7577-7587, 2007.

637   Monks, P. S., Archibald, A. T., Colette, A., Cooper, O., Coyle, M., Derwent, R., Fowler, D., Granier, C., Law, K. S.,
638   Mills, G. E., Stevenson, D. S., Tarasova, O., Thouret, V., von Schneidemesser, E., Sommariva, R., Wild, O.,
639   and Williams, M. L.: Tropospheric ozone and its precursors from the urban to the global scale from air
640   quality to short-lived climate forcer, Atmospheric Chemistry and Physics, 15, 8889-8973, 10.5194/acp-15-
641   8889-2015, 2015.

642   Ordóñez, C., Elguindi, N., Stein, O., Huijnen, V., Flemming, J., Inness, A., Flentje, H., Katragkou, E., Moinat, P.,
643   Peuch, V.-H., Segers, A., Thouret, V., Athier, G., van Weele, M., Zerefos, C. S., Cammas, J.-P., and
644   Schultz, M. G.: Global model simulations of air pollution during the 2003 European heat wave, Atmos.
645   Chem. Phys., 10, 789-815, https://doi.org/10.5194/acp-10-789-2010, 2010.

646   Oikonomakis, E., Aksoyoglu, S., Ciarelli, G., Baltensperger, U., and Prévôt, A. S. H.: Low modeled ozone
647   production suggests underestimation of precursor emissions (especially NOx) in Europe, Atmos. Chem.
648   Phys. Discuss., https://doi.org/10.5194/acp-2017-713, in review, 2017.

649   Pace, G., Meloni, D., and di Sarra, A.: Forest fire aerosol over the Mediterranean basin during summer 2003, J.
650   Geophys. Res., 110, D21202, doi:10.1029/2005JD005986, 2005.

651   Pozzer, A., Jockel, P. J., Sander, R., Williams, J., Ganzeveld, L., and Lelieveld, J.: Technical note: the MESSy-
652   submodel AIRSEA calculating the air-sea exchange of chemical species, Atmospheric Chemistry and
653   Physics, 6, 5435-5444, 2006.

654   Pozzer, A., Jockel, P., Tost, H., Sander, R., Ganzeveld, L., Kerkweg, A., and Lelieveld, J.: Simulating organic
655   species with the global atmospheric chemistry general circulation model ECHAM5/MESSy1: a comparison
656   of model results with observations, Atmospheric Chemistry and Physics, 7, 2527-2550, 2007.

657   Pozzer, A., de Meij, A., Pringle, K. J., Tost, H., Doering, U. M., van Aardenne, J., and Lelieveld, J.: Distributions
658   and regional budgets of aerosols and their precursors simulated with the EMAC chemistry-climate model,
659   Atmospheric Chemistry and Physics, 12, 961-987, 10.5194/acp-12-961-2012, 2012.

660   Pozzer, A., Jöckel, P., and Van Aardenne, J.: The influence of the vertical distribution of emissions on tropospheric
661   chemistry, Atmos. Chem. Phys., 9, 9417–9432, doi:10.5194/acp-9-9417-2009, 2009.

662   Richter, A., Burrows, J. P., Nüss, H., Granier, C., and Niemeier, U.: Increase in tropospheric nitrogen dioxide over
663   China observed from space., Nature, 437, 129-132, 2005.

664   Roeckner, E., Brokopf, R., Esch, M., Giorgetta, M., Hagemann, S., Kornblueh, L., Manzini, E., Schlese, U., and
665   Schulzweida, U.: Sensitivity of simulated climate to horizontal and vertical resolution in the ECHAM5
666   atmosphere model, Journal of Climate, 19, 3771-3791, 10.1175/jcli3824.1, 2006.

667   Sander, R., Baumgaertner, A., Gromov, S., Harder, H., Jöckel, P., Kerkweg, A., Kubistin, D., Regelin, E., Riede, H.,
668   Sandu, A., Taraborrelli, D., Tost, H., and Xie, Z.-Q.: The atmospheric chemistry box model
669   CAABA/MECCA-3.0, Geosci. Model Dev., 4, 373–380, doi:10.5194/gmd-4-373-2011, 2011.

670   Simon, H., Reff, A., Wells, B., Jia, X., and Frank, N.: Ozone Trends Across the United States over a Period of
671   Decreasing NOx and VOC Emissions, Environmental Science & Technology, 49, 186-195, 2015.

672   Solberg, S., Ø. Hov, A. Søvde, I. S. A. Isaksen, P. Coddeville, H. De Backer, C. Forster, Y. Orsolini, and K. Uhse:
673   European surface ozone in the extreme summer 2003, J. Geophys. Res., 113, D07307,
674   doi:10.1029/2007JD009098, 2008

675   Strode, S. A., Rodriguez, J. M., Logan, J. A., Cooper, O. R., Witte, J. C., Lamsal, L. N., Damon, M., Van Aartsen,
676   B., Steenrod, S. D., and Strahan, S. E.: Trends and variability in surface ozone over the United States,
677   Journal of Geophysical Research-Atmospheres, 120, 9020-9042, 10.1002/2014jd022784, 2015.

678   Schultz, M. G., Schroder, S., Lyapina, O., Cooper, O. R., Galbally, I., Petropavlovskikh, I., von Schneidemesser, E.,
679   Tanimoto, H., Elshorbany, Y., Naja, M., Seguel, R. J., Dauert, U., Eckhardt, P., Feigenspan, S., Fiebig, M.,
680   Hjellbrekke, A.-G., Hong, Y.-D., Kjeld, P. C., Koide, H., Lear, G., Tarasick, D., Ueno, M., Wallasch, M.,
681   Baumgardner, D., Chuang, M.-T., Gillett, R., Lee, M., Molloy, S., Moolla, R., Wang, T., Sharps, K.,
682   Adame, J. A., Ancellet, G., Apadula, F., Artaxo, P., Barlasina, M. E., Bogucka, M., Bonasoni, P., Chang, L.,
683   Colomb, A., Cuevas-Agullo, E., Cupeiro, M., Degorska, A., Ding, A., FrHlich, M., Frolova, M., Gadhavi,
684   H., Gheusi, F., Gilge, S., Gonzalez, M. Y., Gros, V., Hamad, S. H., Helmig, D., Henriques, D., Hermansen,
685   O., Holla, R., Hueber, J., Im, U., Jaffe, D. A., Komala, N., Kubistin, D., Lam, K.-S., Laurila, T., Lee, H.,
686   Levy, I., Mazzoleni, C., Mazzoleni, L. R., McClure-Begley, A., Mohamad, M., Murovec, M., Navarro-
687   Comas, M., Nicodim, F., Parrish, D., Read, K. A., Reid, N., Ries, L., Saxena, P., Schwab, J. J., Scorgie, Y.,
688   Senik, I., Simmonds, P., Sinha, V., Skorokhod, A. I., Spain, G., Spangl, W., Spoor, R., Springston, S. R.,
689   Steer, K., Steinbacher, M., Suharguniyawan, E., Torre, P., Trickl, T., Lin, W., Weller, R., Xu, X., Xue, L.,
690   and Ma, Z.: Tropospheric Ozone Assessment Report: Database and metrics data of global surface ozone
691   observations, Elementa-Science of the Anthropocene, 5, 58-Article No.: 58, 10.1525/elementa.244, 2017.

692   Tressol, M., Ordonez, C., Zbinden, R., Brioude, J., Thouret, V., Mari, C., Nedelec, P., Cammas, J.-P., Smit, H., Patz,
693   H.-W., and Volz-Thomas, A.: Air pollution during the 2003 European heat wave as seen by MOZAIC
694   airliners, Atmos. Chem. Phys., 8, 2133-2150, https://doi.org/10.5194/acp-8-2133-2008, 2008.

695   Torseth, K., Aas, W., Breivik, K., Fjaeraa, A.M., Fiebig, M., Hjellbrekke, A.G., Myhre, C.L., Solberg, S., Yttri, K.E.:
696   Introduction to the European Monitoring and Evaluation Programme (EMEP) andobserved atmospheric
697   composition change during 1972–2009. Atmos. Chem. Phys. 12, 5447–5481, 2012

698   Tost, H., Jockel, P. J., and Lelieveld, J.: Lightning and convection parameterisations - uncertainties in global
699   modelling, Atmospheric Chemistry and Physics, 7, 4553-4568, 2007.

700   Weatherhead, E. C., Reinsel, G. C., Tiao, G. C., Meng, X. L., Choi, D. S., Cheang, W. K., Keller, T., DeLuisi, J.,
701   Wuebbles, D. J., Kerr, J. B., Miller, A. J., Oltmans, S. J., and Frederick, J. E.: Factors affecting the detection
702   of trends: Statistical considerations and applications to environmental data, Journal of Geophysical
703   Research-Atmospheres, 103, 17149-17161, 10.1029/98jd00995, 1998.

704   Wilson, R. C., Fleming, Z. L., Monks, P. S., Clain, G., Henne, S., Konovalov, I. B., Szopa, S., and Menut, L.: Have
705   primary emission reduction measures reduced ozone across Europe? An analysis of European rural

706   background ozone trends 1996-2005, Atmospheric Chemistry and Physics, 12, 437-454, 10.5194/acp-12-
707   437-2012, 2012.

708   WHO, 2013 WHO, Review of Evidence on Health Aspects of Air Pollution – REVIHAAP Project, Technical
709   Report World Health Organization, Regional Office for Europe, Copenhagen, Denmark (2013)

710   Yienger, J. J., and Levy, H.: EMPIRICAL-MODEL OF GLOBAL SOIL-BIOGENIC NOX EMISSIONS, Journal of
711   Geophysical Research-Atmospheres, 100, 11447-11464, 10.1029/95jd00370, 1995.

712   Yan, Y., Lin, J., and He, C.: Ozone trends over the United States at different times of day, Atmos. Chem. Phys., 18,
713   1185-1202, https://doi.org/10.5194/acp-18-1185-2018, 2018.

714   Yan, Y., Lin, J., Chen, J., and Hu, L.: Improved simulation of tropospheric ozone by a global-multi-regional two-
715   way coupling model system, Atmospheric Chemistry and Physics, 16, 2381-2400, 10.5194/acp-16-2381-
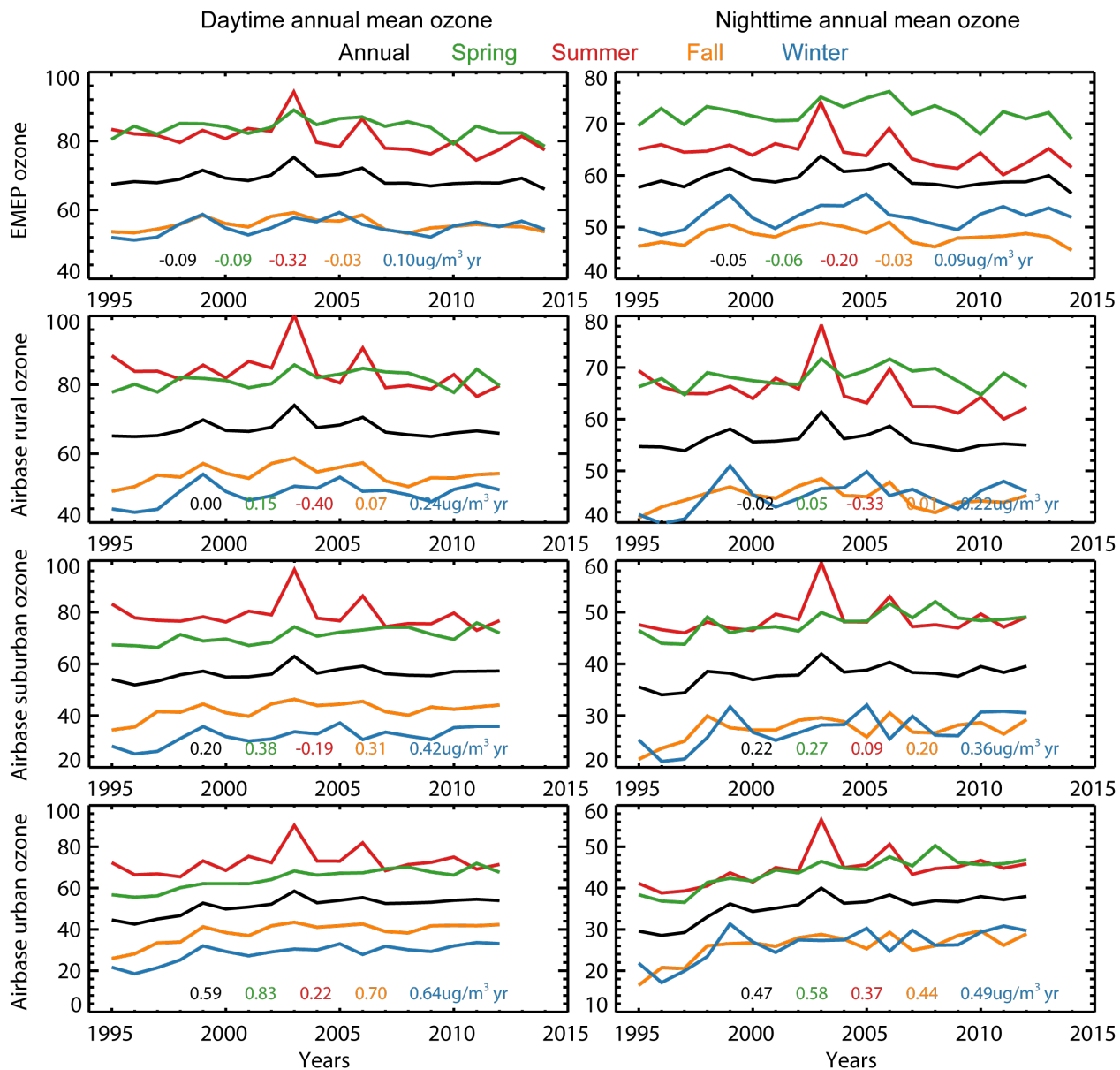716   2016, 2016.

717   Yan, Y. Y., Lin, J. T., Kuang, Y., Yang, D., and Zhang, L.: Tropospheric carbon monoxide over the Pacific during
718   HIPPO: two-way coupled simulation of GEOS-Chem and its multiple nested models, Atmospheric
719   Chemistry and Physics, 14, 12649-12663, 10.5194/acp-14-12649-2014, 2014.

720   Yoon, J., and Pozzer, A.: Model-simulated trend of surface carbon monoxide for the 2001-2010 decade, Atmospheric
721   Chemistry and Physics, 14, 10465-10482, 10.5194/acp-14-10465-2014, 2014.

722
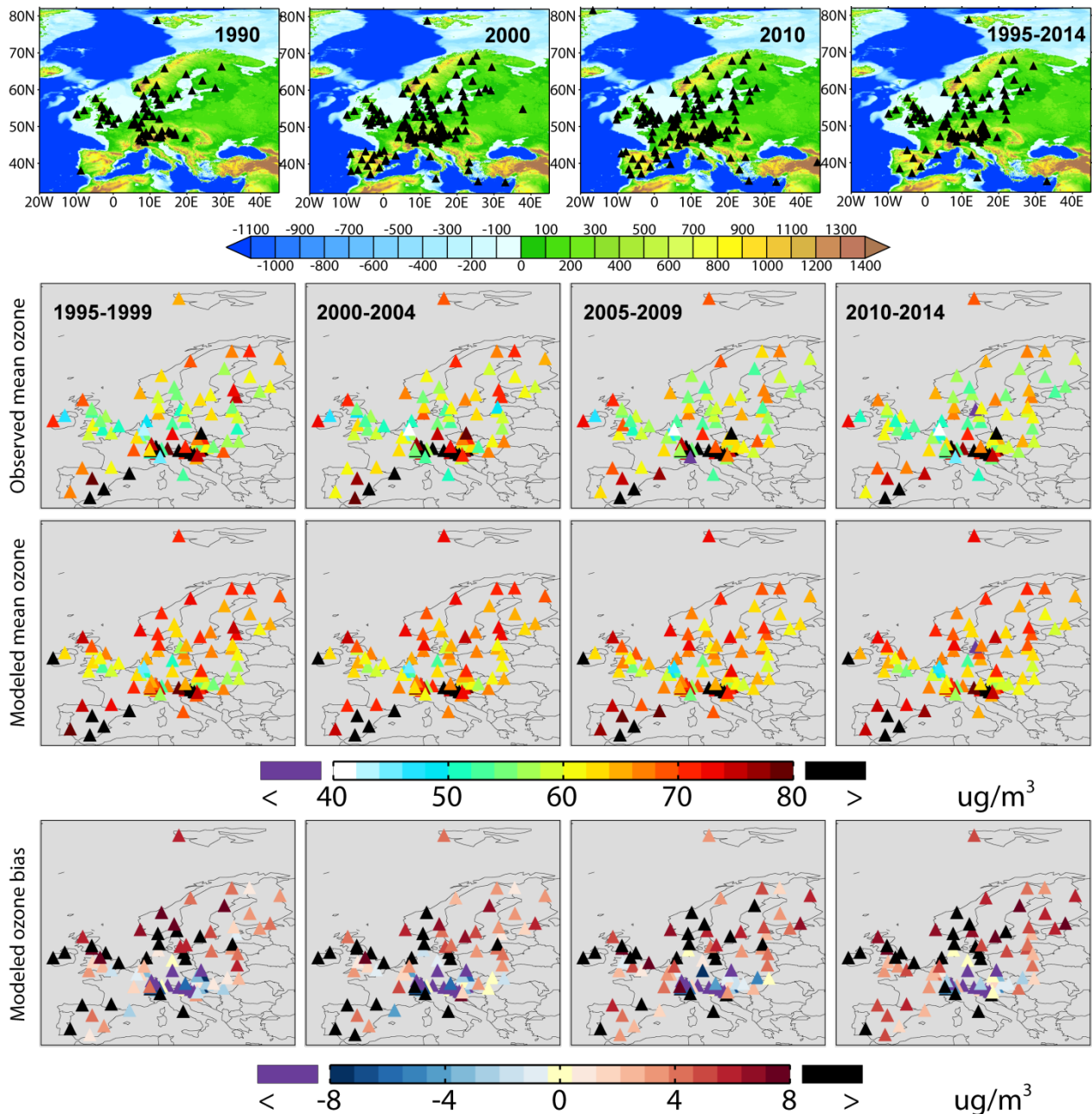
723
724 Fig. 1. Site distribution (first row) for the EMEP datasets (1990, 2000, 2010) as well as the selected 93 sites (1995-
725 2014). The overlaid map shows the surface elevation (m) from a 2 min Gridded Global Relief Data (ETOPO2v2)
726 available at NGDC Marine Trackline Geophysical database (http://www.ngdc.noaa.gov/mgg/global/etopo2.html).
727 The observed (second row) and modeled (third row) mean ozone mixing ratios, and also the modeled ozone biases
728 for every five years during 1995-2014 over the selected 93 sites are shown below.
729

730

Fig. 2 Annual and seasonal mean daytime and nighttime ozone mixing ratios averaged over the selected sites for EMEP network (first row) as well as Airbase network (second row for Airbase rural sites; third row for Airbase suburban sites; forth row for Airbase urban sites). Also shown in each panel are the trends.
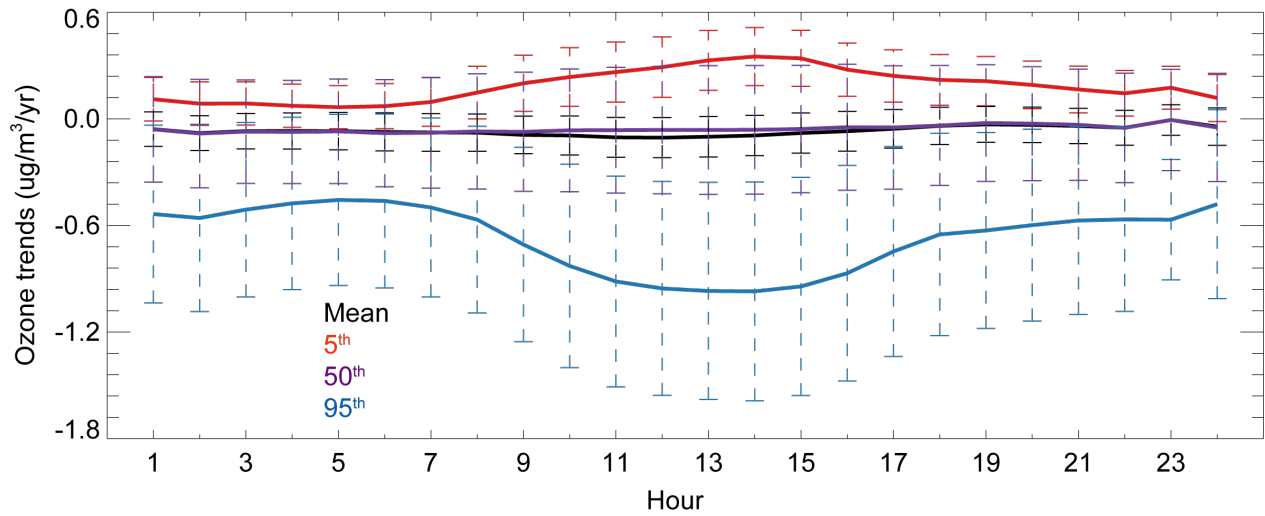
Fig. 3. Trend in the observed surface ozone averaged over Europe, calculated for the selected 93 sites. The black line shows the 1995–2014 linear trends in the deseasonalized European monthly ozone anomalies for each hour of the day (local standard time), the red, purple and blue lines depict the observed trend for 5th, 50th and 95th percentile ozone, respectively, and the dashed bars indicate their standard deviations.

741

742
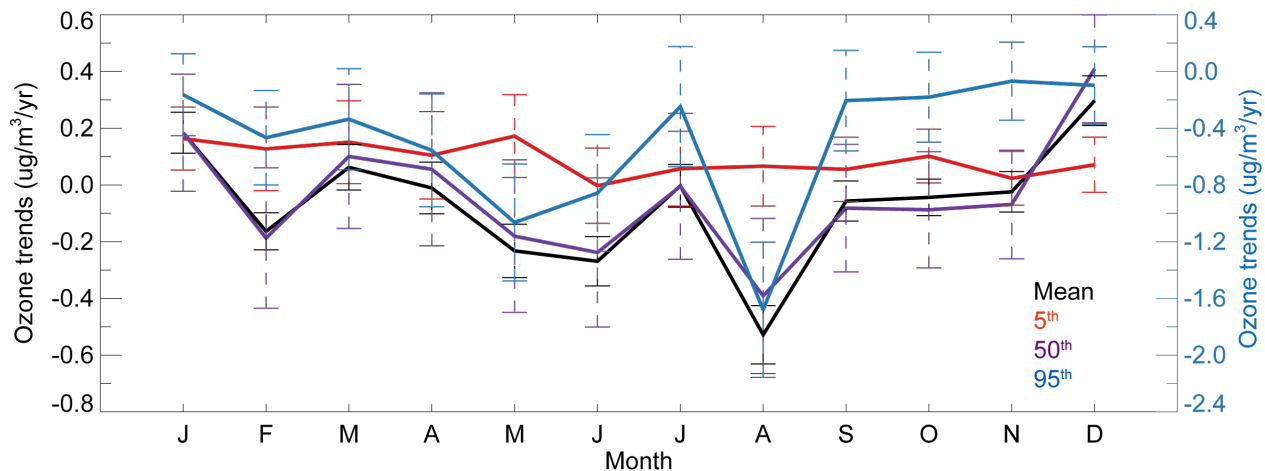
743 Fig. 4. Monthly trend in the observed surface ozone averaged over Europe for the selected 93 sites. The black line
744 shows the 1995–2014 linear trends in the European mean ozone for each month of the year, the red, purple and blue
745 lines depict the observed trend for 5th, 50th and 95th percentile ozone, respectively, and the dashed bars indicate their
746 standard deviations. The left axis is for the trends of mean, 5th, and 50th percentile ozone, while the right axis for the
747 95th percentile ozone.

748

749

750
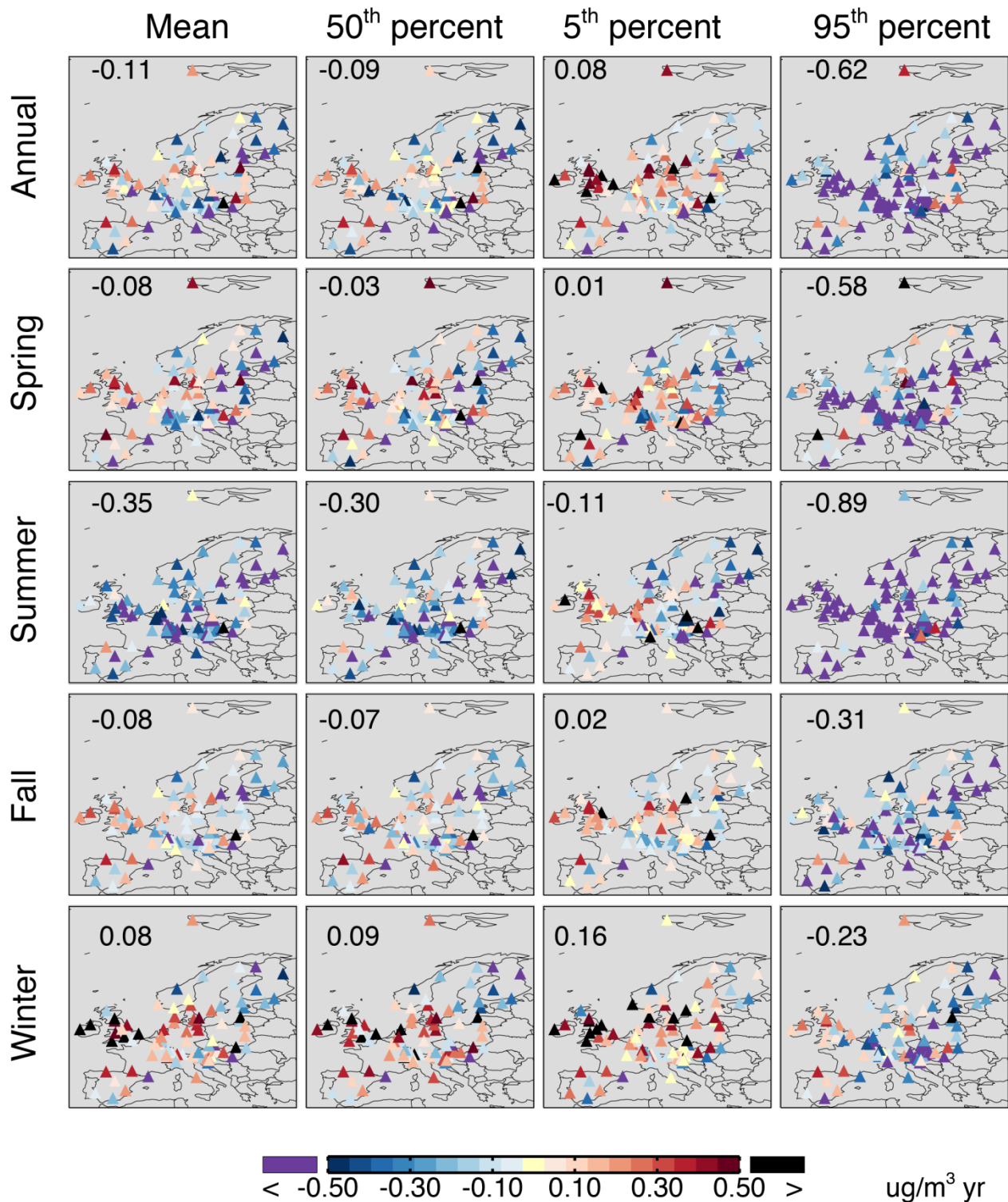

Fig. 5. Spatial distribution of measured daytime ozone trends in µg/m³/yr across the selected 93 sites for average, 5th, 50th and 95th percentile ozone in annual mean and four seasons. Also shown in each panel are the average trends over all sites.

751
752
753
754
755
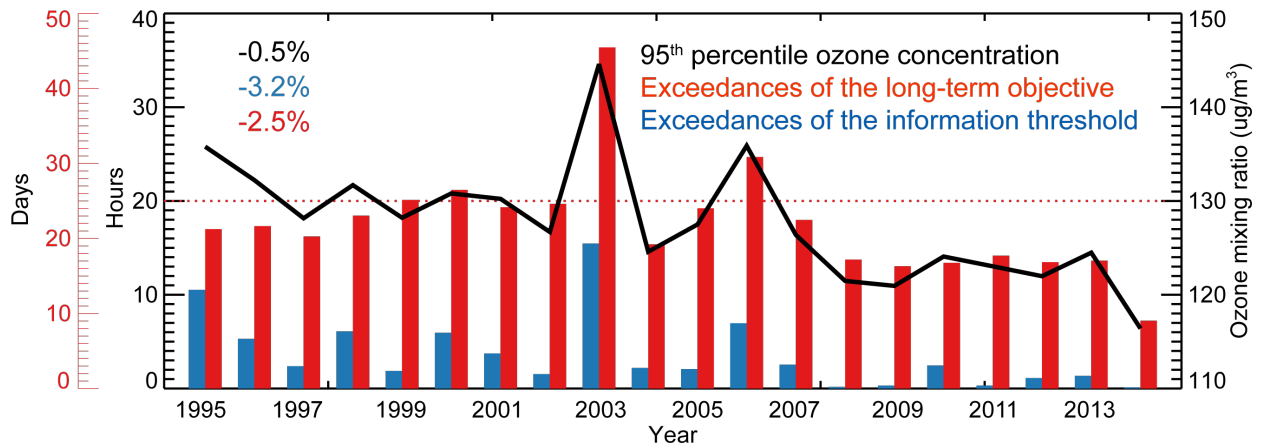
756
757 Fig. 6. Annual exceedances of the information threshold (for blue bars, hours should be multiplied by 100, 1-hourly
758 averages: 180 μg/m^3) as well as the long-term objective (red bars, maximum diurnal 8-hourly mean: 120 μg/m^3),
759 compared with the annual 95th percentile ozone concentrations (black line). Red dotted line shows the target value
760 (long-term objective that should not be exceeded more than 25 days per year, averaged over 3 years).
761
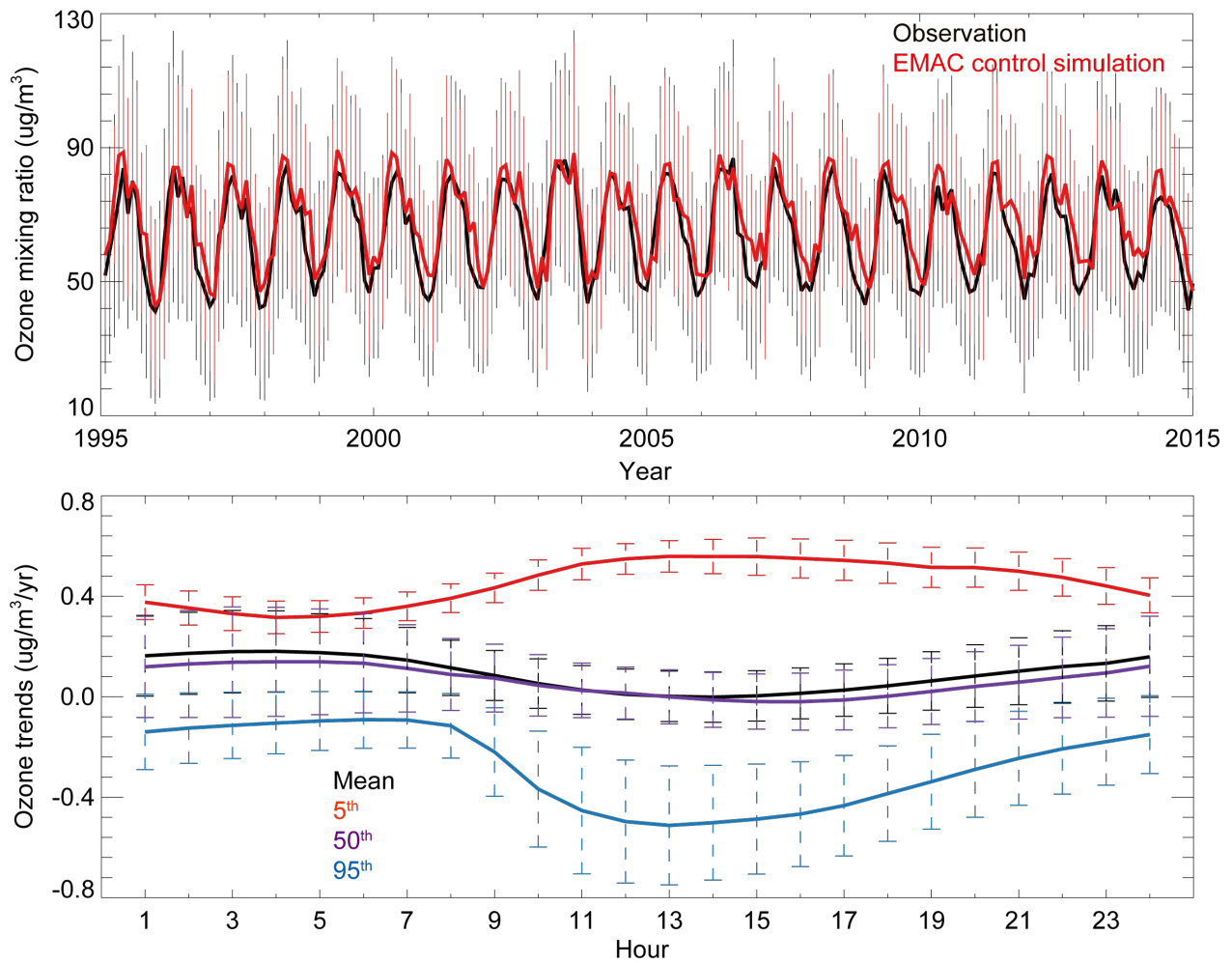
Fig. 7. EMAC modeled ozone in μg/m³ over Europe during 1995-2014. Time series of measured (black) and modeled (red) monthly mean ozone over the 93 selected sites (top). Trend in the modeled surface ozone averaged over the selected 93 sites for all hours of the day (local time, bottom). The black line shows the 1995-2014 linear trends in the European mean ozone, the red, purple, and blue lines are the modeled trends for 5th, 50th and 95th percentile ozone, respectively. The dashed bars indicate their standard deviations.
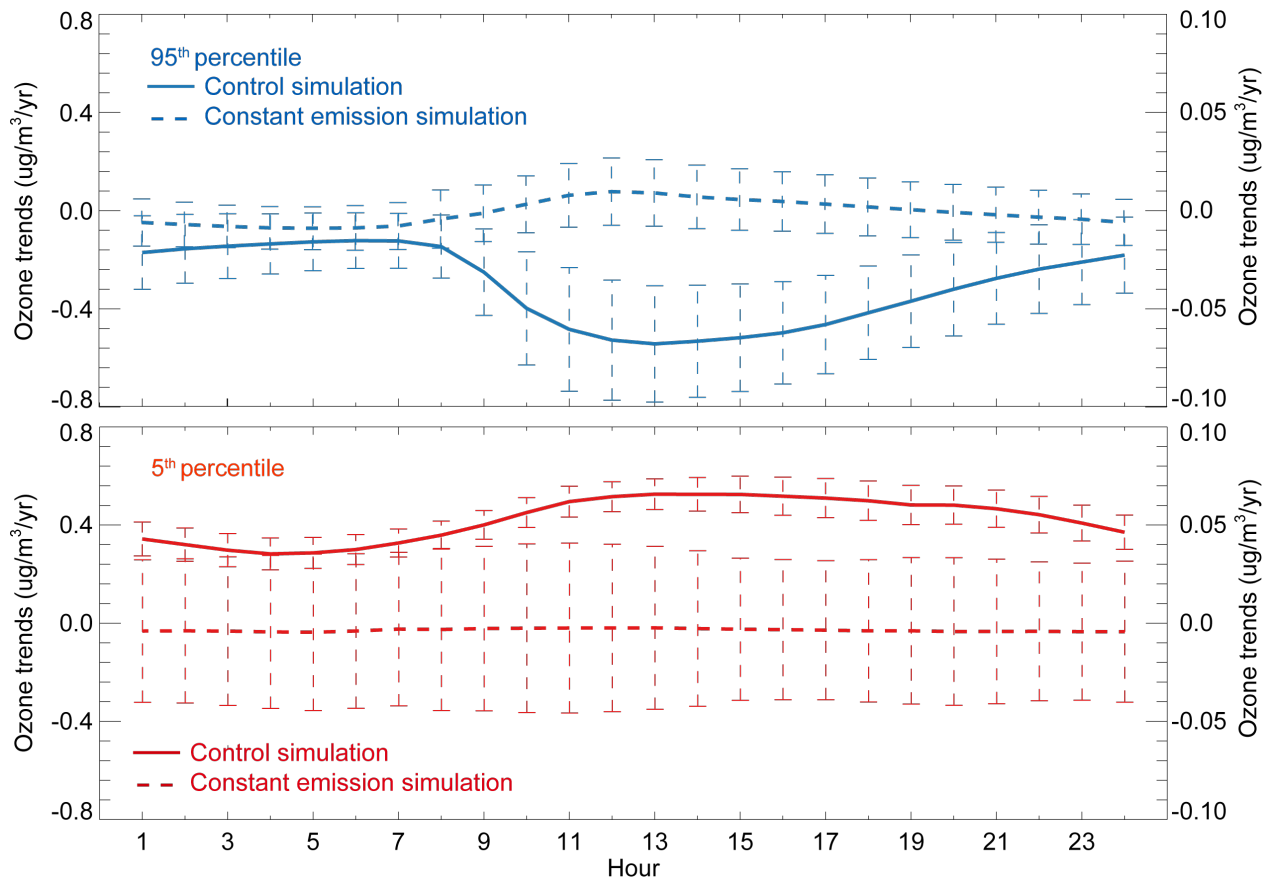
Fig. 8. Modeled trend in the surface ozone averaged over the selected 93 sites for all hours of the day (local time). The solid lines (left legends) show the 1995-2014 linear trends in the control simulation for 95th (top) and 5th percentile (bottom) ozone, respectively. The dashed lines (right legends) represent the modeled trends by the constant emission simulation. The bars indicate their deviations.

776
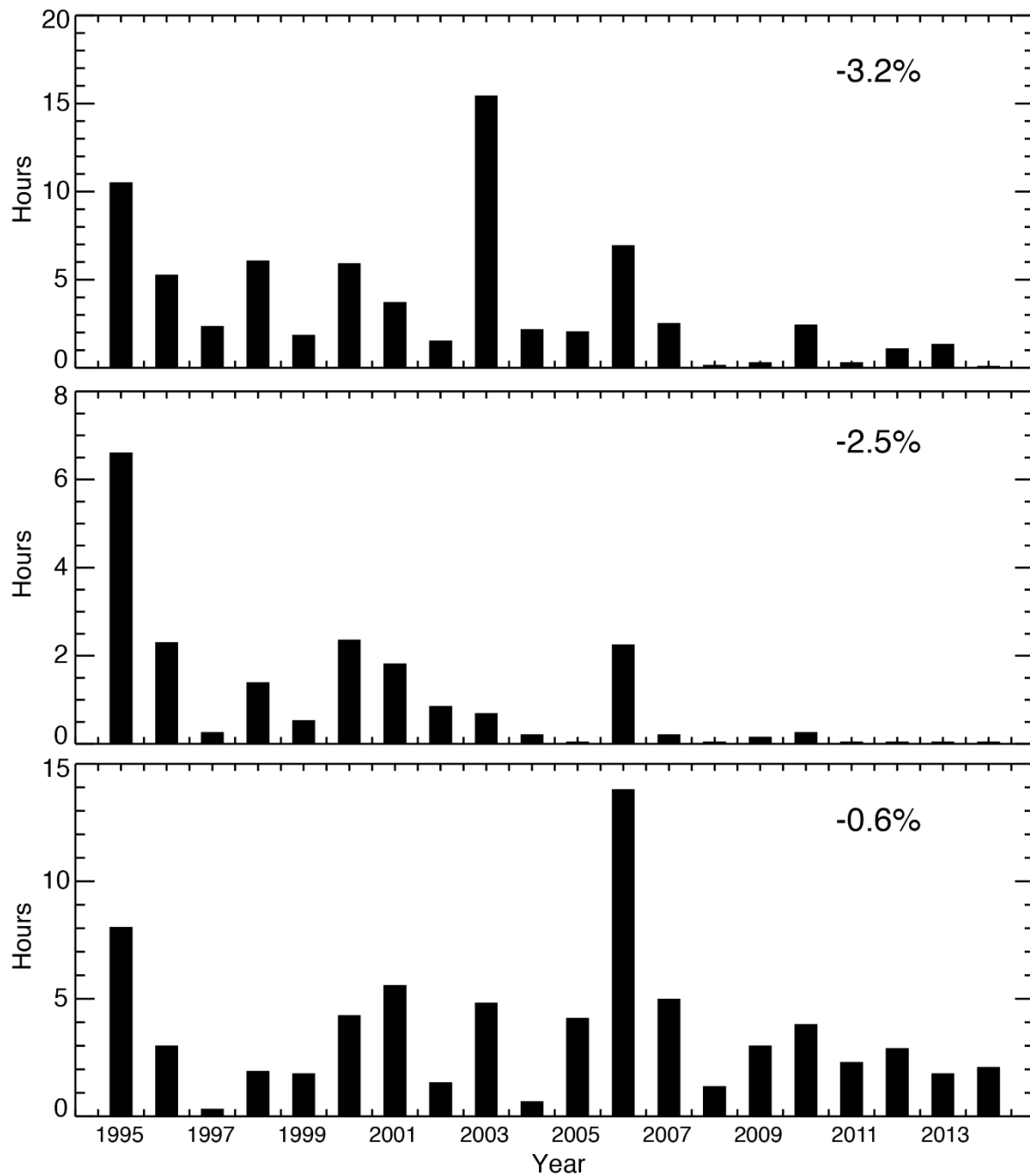
777
778 Fig. 9. Annual observed (top) and modeled (middle: control simulation; bottom: constant emission simulation)
779 exceedances of the information threshold (1-hourly averages: 180 μg/m³). The hours along the y-axis should be
780 multiplied by 100.
781

782

Information threshold Long-term objective 2 meter temperature

783
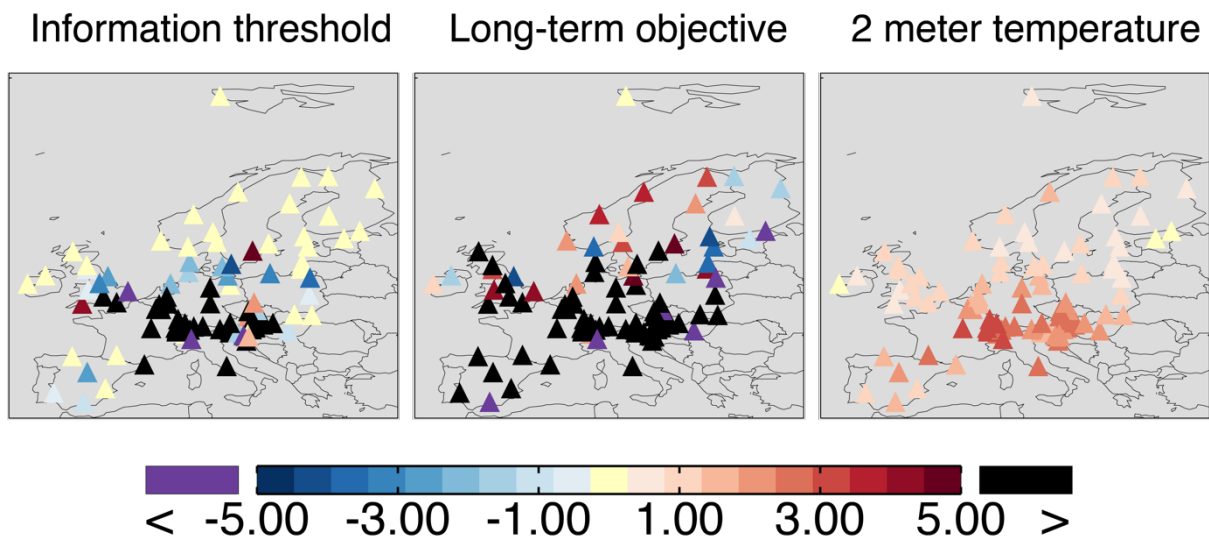
Fig. 10. Spatial distribution of the exceedance anomalies in 2003, relevant to the averages over 1995-2002 and for the information threshold as well as the long-term objective, in comparison with the 2-meter temperature anomalies in each of the sites.

787
788

789
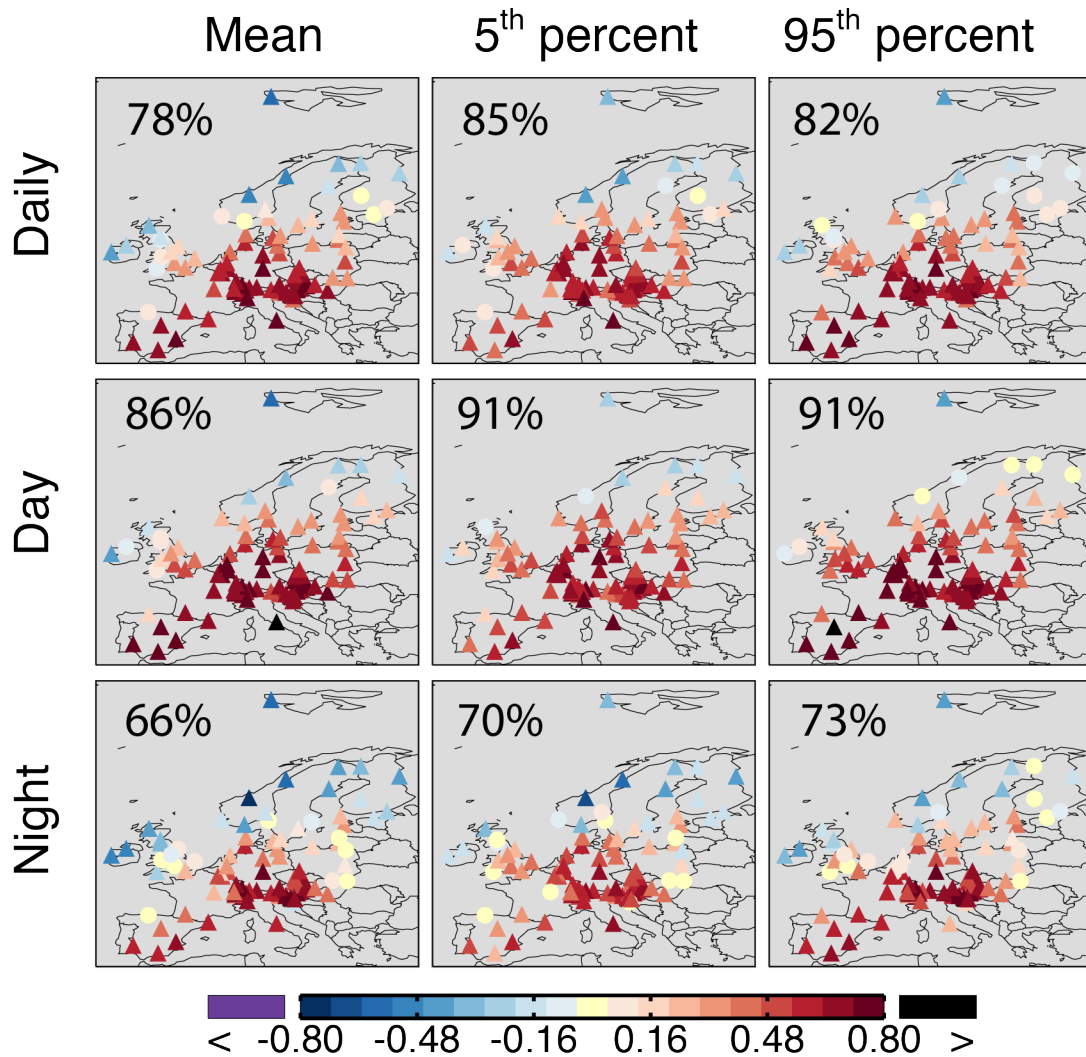
Fig. 11. Site-by-site correlations (triangle: P-value < 0.05 under a *T*-test; circular: P-value > 0.05) between the monthly mean 2-meter temperature and monthly mean, 5th and 95th percentile ozone in the daily data, and during daytime as well as nighttime. Also shown in each panel are the fraction of sites for which significant correlation exists.

790
791
792
793
794
795
796
797

798   Table 1. Percentage of missing hourly data in each year in the EMEP station observations.

Year	Number of sites	Missing data		
		Whole day	Daytime	Nighttime
1995	113	32.6%	30.6%	34.6%
1996	115	28.8%	26.7%	30.9%
1997	121	23.9%	21.6%	26.2%
1998	120	18.5%	16.0%	21.0%
1999	127	10.4%	7.9%	12.8%
2000	132	9.8%	7.2%	12.3%
2001	134	11.9%	9.4%	14.4%
2002	136	9.3%	6.8%	11.8%
2003	137	12.1%	9.8%	14.4%
2004	135	10.9%	8.5%	13.3%
2005	132	10.5%	8.1%	12.9%
2006	130	10.6%	8.1%	13.1%
2007	132	9.5%	7.0%	12.0%
2008	136	10.8%	8.2%	13.4%
2009	134	10.6%	7.8%	13.3%
2010	136	15.0%	12.6%	17.5%
2011	135	13.8%	11.4%	16.2%
2012	136	14.1%	11.8%	16.4%
2013	136	19.9%	17.8%	22.0%
2014	137	21.0%	19.1%	23.0%

799
800

801 Table 2. Modeled and observed ozone trends[1] and their standard deviations based on diurnal
802 average European mean ozone concentrations. The mean, 5th, 50th, and 95th percentile represent
803 the monthly statistics of the diurnal averages. The model has been sampled in the same location
804 of the EMEP stations.

	5th percentile	50th percentile	Mean	95th percentile
EMEP ($\mu g/m^3/y$)	$0.22^{**} \pm 0.15$	-0.05 ± 0.23	-0.07 ± 0.21	$-0.57^{**} \pm 0.34$
EMAC ($\mu g/m^3/y$)	$0.42^{**} \pm 0.14$	0.01 ± 0.10	0.06 ± 0.09	$-0.23^{**} \pm 0.10$

805 1. ** P-value < 0.01. * P-value < 0.05 under an *F*-test.
806

808 Table 3. Modeled and observed linear trends[1] and their spatial standard deviations of the 1995–
809 2014 European mean annual and seasonal averaged daytime and nighttime mean as well as their
810 5th, 50th and 95th percentile ozone concentrations (averaged over the 93 sites).

811

	Seasons	Mean		5th percentile		50th percentile		95th percentile	
		EMEP	EMAC	EMEP	EMAC	EMEP	EMAC	EMEP	EMAC
Daytime (μg/m^3/y)	Annual	-0.09± 0.24	0.00± 0.06	0.22** ±0.17	0.45** ±0.14	-0.06± 0.24	-0.01± 0.06	-0.81** ±0.46	-0.48** ±0.15
	MAM	-0.09± 0.27	-0.05± 0.08	0.13± 0.24	0.52** ±0.17	-0.02± 0.27	-0.02± 0.08	-0.93** ±0.53	-0.49** ±0.16
	JJA	-0.32** ±0.24	-0.10± 0.07	-0.03± 0.26	0.41** ±0.20	-0.26** ±0.24	-0.09± 0.13	-1.10** ±0.61	-0.54** ±0.16
	SON	-0.03± 0.19	-0.04± 0.05	0.09± 0.14	0.36** ±0.12	-0.04± 0.20	-0.02± 0.05	-0.24** ±0.25	-0.44** ±0.23
	DJF	0.10± 0.25	0.18** ±0.14	0.25** ±0.15	0.39** ±0.22	0.05± 0.27	0.15*± 0.20	-0.28** ±0.31	-0.08± 0.05
Nighttime (μg/m^3/y)	Annual	-0.05± 0.23	0.12*± 0.11	0.16*± 0.17	0.38** ±0.19	-0.05± 0.24	0.07± 0.12	-0.57** ±0.36	-0.21** ±0.10
	MAM	-0.06± 0.29	0.08± 0.10	0.18*± 0.23	0.23** ±0.23	-0.00± 0.29	0.04± 0.08	-0.64** ±0.43	-0.20** ±0.12
	JJA	-0.20* ±0.27	0.06± 0.14	0.07± 0.24	0.36** ±0.22	-0.15± 0.28	0.04± 0.14	-0.71** ±0.52	-0.36** ±0.21
	SON	-0.03± 0.21	0.06± 0.10	0.05± 0.12	0.19** ±0.16	-0.05± 0.23	0.04± 0.11	-0.21* ±0.24	-0.23** ±0.19
	DJF	0.09± 0.24	0.24** ±0.18	0.14± 0.22	0.43** ±0.27	0.06± 0.25	0.20*± 0.25	-0.24* ±0.29	-0.05± 0.06

812   1.   ** P-value < 0.01. * P-value < 0.05 under an *F*-test.

813